UNIVERSITY OF CALIFORNIA, SAN DIEGO

Particle-Based Vaccination through Direct Targeting of Antigen Presenting Cells

A dissertation submitted in partial satisfaction of the requirements for the degree Doctor of Philosophy

in

Biomedical Sciences

by

Laura E. Ruff

Committee in charge:

Professor Stephen M. Hedrick, Chair
Professor Maripat Corr
Professor Shane Crotty
Professor Victor Nizet
Professor Elina I. Zuniga

2012

The Dissertation of Laura E. Ruff is approved, and it is acceptable in quality and form for publication on microfilm and electronically:

_____

_____

_____

_____

_____

Chair

University of California, San Diego

2012

TABLE OF CONTENTS

Signature Page. iii

Table of Contents. iv

List of Figures. v

Acknowledgements. vii

Vita. x

Abstract of the Dissertation. xii

Chapter I
Introduction. 1

Chapter II
Antigen-loaded pH-sensitive hydrogel microparticles are taken up by dendritic cells with no requirement for targeting antibodies. 18

Chapter III
Multivalent porous silicon nanoparticles enhance the immune activation potency of agonistic CD40 antibody. 49

Chapter IV
Discussion. 90

References. 94

LIST OF FIGURES

Chapter II

Figure 1. Antibodies can be conjugated to pH-sensitive hydrogel microparticles and maintain binding activity. 38

Figure 2. Co-culture with microparticle-treated BMDCs produced CD8 and CD4 proliferation *in vitro*. 39

Figure 3. All microparticles, regardless of antibody conjugation, induce upregulation of CD80 and CD86 on BMDCs. 40

Figure 4. Fluorescent particles recruit neutrophils and monocytes to the draining LN. 42

Figure 5. Secondary immune response to VSV-OVA challenge. 43

Figure 6. ^{1}H NMR of acid-sensitive crosslinker. 47

Chapter III

Figure 1. Preparation and characterization of FGK45 loaded luminescent porous silicon nanoparticles (FGK-LPSiNP). 65

Figure 2. Dendritic cell uptake of FGK-LPSiNPs. 66

Figure 3. Interaction of FGK-LPSiNPs with B cells. 67

Figure 4. Amplified activation potency of FGK-LPSiNPs compared to free FGK45. 68

Figure 5. Immunoblot analysis of FGK45 loaded on luminescent porous silicon nanoparticles (LPSiNPs). 72

Figure 6. Representative hydrodynamic size data. 73

Figure 7. Dendritic cell uptake of FGK-LPSiNPs. 74

Figure 8. Photoluminescence spectra of LPSiNPs in acidic buffer solutions at room temperature. 75

Figure 9. Stimulation of B cells using various concentrations of FGK45 loaded LPSiNPs. 76

Figure 10. No CD86 or MHC II upregulation of B cells incubated with LPSiNP. 77

Figure 11. Antibody-OVA constructs. 85

Figure 12. Antibody-OVA LPSiNP constructs *in vitro*. 86

Figure 13. Antibody-OVA LPSiNP constructs *in vivo*. 87

ACKNOWLEDGEMENTS

I'll start out thanking my family. I've known you all for 32 years, right? Matching Christmas dresses, first day of school pictures, cartwheels in the living room, Marianne and I in London, Kristy and I at Wrigley Field, family trip to Disneyworld (and just last year to Disneyland). Thanks for being a model family. Thanks to my husband, Tommy. He doesn't let things bother him like I do, and there have been a million times he has let me cancel plans, have my way, or win an argument to keep me from going crazy, even though I steal all his chocolate.

There have been many people in the Hedrick lab, past and present, who have helped me, provided a laugh, or a beer. I'll start with Carol, our lab manager, lab mom, and chef extraordinaire. She started work on what would become my thesis project years before I started, so thanks for that, or I would still be years from graduating. Irene, haircut, breakfast, and 'gym' buddy. Bryce, favorite complaining buddy and partner in negative data. Kevin, fan of all obtuse facts and ACK buffer saboteur. Fang, grad school commiserator. Warren, Simon & Garfunkel Fridays. Anne, who didn't understand a word I said. Jenn, fun facts about St. Louis. There have been many others, who I've shared a glass of wine, beer, or bread and cheese for a paper, grant, happy hour, or power outage. Then there are members of the Murre and Goldrath labs, particularly the Murre-maids, Amanda, Elinore, Claudia, Marty, Eva,

Susanne, Kristina, and Mandy, and the Gophers, Louise, Kitty, and Adam. You've always made me feel welcome, even though I mostly just steal your antibodies. Thanks to Maripat Corr, who seems to know about everything, and who met with us every month for years and saw a lot of negative data. Finally, the boss, Steve Hedrick, who always has free-flowing advice, provides an excellent work environment, allows one freedom to pursue the direction on their project that they choose, and always has ideas for experiments involving sheep red blood cells.

Thanks also go to my fellow grad student friends. Out of a class of 18, I will be the 17th to defend my thesis. The 18th is still here too, with plans to defend in a few months. So kudos to everybody, I think that is pretty cool that we all made it to Ph.D., with no dropouts or terminal masters. Especially thanks to Morgan, Nisha, Robert (Bobs), Lori, Audrey, Molly, John, Edoardo (Eds), and Derina, for Saturday night dinners, Ph.D. pity parties, camping and hiking adventures, and an occasional just plain old trip to the bar.

I'm not sure how many people actually read this section, except for some poor graduate students many years after the fact, who find themselves reading an old thesis from their lab to figure out how the heck this thing is supposed to be formatted. So thanks, Dan Beisner and Ben Wen, imitation (but strictly in the formatting sense here) is the sincerest form of flattery.

The text of Chapters II, in full, has been submitted for publication. I was the primary researcher and author and the co-authors, Enas A. Mahmoud,

Jagadis Sankaranarayanan, José M. Morachis, Carol D. Katayama, Maripat Corr, Stephen M. Hedrick, and Adah Almutairi, directed and supervised the research which forms the basis for this chapter.

The Text of Chapter III, in part, has been submitted for publication. I was the secondary researcher and author, and the co-authors, Luo Gu, Zhengtao Qin, Maripat Corr, Stephen M. Hedrick, and Michael J. Sailor, directed and supervised the research which forms the basis for this chapter.

VITA

1998-2001	Student Lab Animal Technician, University of Minnesota, Twin Cities (Advisor, Dr. Laura Mauro)
2000-2001	Directed Research, University of Minnesota, Twin Cities (Advisor, Dr. Amy P.N. Skubitz)
1998-2001	B.S., Microbiology, University of Minnesota, Twin Cities
2001	Junior Scientist, University of Minnesota, Twin Cities (Advisor, Dr. Laura Mauro)
2001-2005	Biologist, Vaccine Research Center, National Institutes of Health (Advisor, Dr. Daniel Douek)
2005-2012	Ph.D., Biomedical Sciences, University of California, San Diego (Advisor, Dr. Stephen Hedrick)

Publications

Antigen-loaded pH-sensitive hydrogel microparticles are taken up by dendritic cells with no requirement for targeting antibodies. **Ruff LE**, Mahmoud EA, Sankaranarayanan J, Morachis JM, Katayama CD, Corr M, Hedrick SM, Almutairi A. [In preparation].

Multivalent porous silicon nanoparticles enhance the immune activation potency of agonistic CD40 antibody. Gu L, **Ruff LE**, Qin Z, Corr M, Hedrick SM, Sailor MJ. [In preparation].

*HLA B*5701+ long-term nonprogressors/elite controllers are not distinguished from progressors by the clonal composition of HIV-specific CD8+ T-cells.* Mendoza D, Royce C, **Ruff LE**, Ambrozak DR, Quigley M, Dang T, Venturi V, Price DA, Douek DC, Migueles SA, Connors M. J Virology. 2012 Jan 25 [Epub ahead of print].

High functional avidity CTL responses to HLA-B-restricted Gag-derived epitopes associate with relative HIV control. Berger CT, Frahm N, Price DA, Mothe B, Ghebremichael M, Hartman K, Henry LM, Brenchley JM, **Ruff LE**, Venturi V, Pereyra F, Sidney J, Sette A, Douek DC, Walker BD, Kaufmann DE, Brander C. J Virology. 2011 Sept; 85(18):9334-45.

Acquisition of direct antiviral effector functions by CMV specific CD4+ T lymphocytes with cellular maturation. Casazza JP, Betts MR, Price DA, Precopio ML, **Ruff LE**, Brenchley JM, Hill BJ, Roederer M, Douek DC, Koup RA. J Exp Med. 2006 Dec 25;203(13):2865-77.

Preferential infection shortens the life span of Human Immunodeficiency Virus-specific CD4+ T cells in vivo. Brenchley JM, **Ruff LE**, Casazza JP, Koup RA, Price DA, Douek DC. J Virology. 2006 July; 80(14):6801-6809.

Avidity for antigen regulates clonal hierarchies in CD8+ T cell populations specific for persistent DNA viruses. Price DA, Brenchley JM, **Ruff LE**, Betts MR, Hill BJ, Roederer M, Koup RA, Migueles S, Gostick E, Wooldridge L, Sewell AK, Connors M, Douek DC. J Exp Med. 2005 Nov 21;202(10):1349-61.

T-cell receptor recognition motifs govern immune escape patterns in acute SIV infection. Price DA, West SM, Betts MR, **Ruff LE**, Brenchley JM, Ambrozak DR, Edghill-Smith Y, Kuroda MJ, Bogdan D, Kunstman| K, Letvin NL, Wolinsky| SM, Franchini G, Koup RA, Douek DC. Immunity. 2004 Dec;21(6):793-803.

CD4+ T cell depletion during all stages of HIV disease occurs predominantly in the gastrointestinal tract. Brenchley JM, Schacker TW, **Ruff LE**, Price DA, Taylor JH, Beilman GJ, Nguyen PL, Khoruts A, Larson M, Haase AT, Douek DC. J Exp Med. 2004 Sep 20;200(6):749-59.

Definitive separation of graft-versus-leukemia- and graft-versus-host-specific CD4+ T cells by virtue of their receptor beta loci sequences. Michalek J, Collins RH, Durrani HP, Vaclavkova P, **Ruff LE**, Douek DC, Vitetta ES. Proc Natl Acad Sci U S A. 2003 Feb 4;100(3):1180-4.

Beta 1-integrins regulate the formation and adhesion of ovarian carcinoma multicellular spheroids. Casey RC, Burleson KM, Skubitz KM, Pambuccian SE, Oegema TR, **Ruff LE**, Skubitz APN. American Journal of Pathology 2001 Dec;159(6):2071-80.

ABSTRACT OF THE DISSERTATION

Particle-Based Vaccination through Direct Targeting of Antigen Presenting Cells

by

Laura E. Ruff

Doctor of Philosophy in Biomedical Sciences

University of California, San Diego, 2012

Professor Stephen M. Hedrick, Chair

Particle-based delivery of antigen has great potential for generating improved vaccines. During the course of an immune response, a pathogen may trigger multiple pattern-recognition receptors, instilling a strong proinflammatory immune response. Highly successful vaccines, such yellow fever vaccine and Dryvax® (smallpox), also induce immune responses by

utilizing multiple pathogen-sensing signaling pathways, yielding long-lasting B and T cell responses. Subunit vaccines generally require an external adjuvant to boost immune responses; however, recent data has shown that targeting multiple immune activation pathways generates a more potent immune response, similar to native infection or immunization with live vaccines (Kasturi et al., 2011; Ahonen et al., 2004, 2008).

To determine the effects of presenting targeting and/or activating moieties in a multivalent form, we generated two different particle-based vaccines. The first, an antigen-loaded, pH-sensitive hydrogel microparticle, was found to be taken up and presented by bone marrow-derived dendritic cells (BMDCs) *in vitro* and targeted to dendritic cells (DCs) and monocytes *in vivo*. Addition of targeting antibodies to the particle surface did not influence its uptake. DCs also upregulated activation markers when treated with microparticles, even when no agonistic anti-CD40 was conjugated to the microparticles. Furthermore, these particles induced increased percentages of interferon-ɣ-producing CD8 T cells in response to challenge with a pathogen expressing the same antigen, in both an accelerated vaccination strategy using pre-loaded BMDCs and a traditional mouse immunization setting.

The second particle, a luminescent porous silicon nanoparticle, displayed the same targeting and/or activating antibodies. This particle used antigen that was encoded in the 3' end of the targeting antibody instead of encapsulating it in the particle. Nanoparticles displaying agonistic anti-CD40

(with no antigen), produced a multivalent effect in B cells *in vitro*, in which the stimulatory effects of the CD40 nanoparticle were observed at 30-40-fold lower dose of antibody versus free anti-CD40. *In vitro* and *in vivo*, nanoparticles displaying targeting antibodies induced CD8 T cell proliferation better than those displaying control antibodies; however, this effect could not be consistently observed long-term *in vivo*, even with both targeting antibody and anti-CD40. In fact antigen-specific cells were most often deleted at memory time points.

Chapter I

Introduction

1. Antigen Presenting Cells

1.1. Dendritic cells

Dendritic cells (DCs) are the premier antigen presenting cells (APCs) of the body, able to induce both innate and adaptive immune effectors through coreceptor stimulation, antigen presentation, and cytokine/chemokine production. They are able to take up, process, and present antigen from viral, bacterial, fungal, parasitic, and self sources. DCs present peptides in the context of major histocompatibility class I (MHC I) or class II (MHC II) to CD8 and CD4 T cells, respectively. Furthermore, mature DCs are able to migrate to secondary lymphoid sites and activate the appropriate downstream effectors to combat each specific type of pathogen. When DCs were deleted in an inducible mouse model, CD8+ T cells failed to respond to *Listeria monocytogenes* and *Plasmodium yoelii*, two intracellular pathogens (Jung et al., 2002). If DCs were deleted upon secondary infection, fewer memory CD8+ T cells responded to *Listeria*, vesicular stomatitis virus (VSV), or influenza virus (Zammit et al., 2005).

In addition to activating responses, DCs can also induce tolerance to antigen due to insufficient costimulation or lack of antigen presentation. In vaccination experiments targeting antigen to DEC205, an endocytic receptor primarily expressed by DCs, T cells were tolerized to the antigen unless costimulation in the form of agonistic anti-CD40 was given concurrently (Hawiger et al., 2001; Bonifaz et al., 2002). In the case of poorly immunogenic

tumors, CD8+ T cells were still induced to respond by DCs, but underwent poor clonal expansion and were functionally impaired, leading to tolerance instead of activation, resulting in tumor progression (Gerner et al., 2008; Curtsinger et al., 2007; Lyman et al., 2004; Anderson et al., 2007). This was partly due to lack of help from CD4+ T cells, which did not respond because no tumor antigens were presented on MHC II by DCs (Gerner et al., 2008). Thus, DCs are central to induction of a productive immune response, due to their ability to influence multiple immune effectors.

1.1.1. Types of DCs in mice

As immune sentinels, one place DCs are found is in the tissues exposed to the external environment. Four types of DCs have been identified: conventional (cDCs)—which can be further subdivided into migratory DCs and lymphoid-resident DCs, Langerhans cells (LCs), plasmacytoid DCs (pDCs), and inflammatory DCs or monocyte-derived DCs (moDCs).

cDC progenitors are produced in the bone marrow. Pre-cDCs migrate from the bone marrow through the blood to non-hematopoietic tissues and secondary lymphoid organs. The cDCs in the tissue, such as the dermis and gut, are the migratory subset, and they express CD11b or CD103 (Belz et al., 2004; Bedoui et al., 2009). These cells migrate to the lymph nodes to present antigen. The lymphoid-resident cDCs reside in the lymph nodes and the spleen. These cells can be categorized as CD8α+ or CD8α-. The CD8 consists of two α chains, as opposed to CD8 expressed by T cells, which is

made up of an α and a β chain. CD8α+ DCs are the primary DCs found in the thymus, though they are also present to lesser degrees in lymph nodes and spleen. They also express DEC205, a C-type lectin receptor, and are specialized at presentation of antigen on MHC I (Bonifaz et al., 2002; den Haan et al., 2000). These DEC205+CD8α+ DCs reside in the T cell areas of the spleen as well as the lymph nodes. CD8α- DCs are primarily found in the spleen and lymph nodes. These cells express DC inhibitory receptor 2 (DCIR-2), which directs antigens to the MHC class II pathway (Dudziak et al., 2007). In addition, the DCIR-2+CD8α- DCs reside in the marginal zone and red pulp of the spleen (Dudziak et al., 2007).

LCs do not arise from a bone marrow precursor, as all other DC subsets do. Their precursor population is a macrophage population that is present during embryonic development and undergoes a proliferative burst shortly after birth (Chorro et al., 2009). LCs express the C-type lectin receptor langerin, are found in the epidermis, and like migratory cDCs, they migrate to the lymph nodes to present antigen. Other DC subsets have recently been shown to express langerin also, muddying the research done on this DC subset (Bursch et al., 2007; Ginhoux et al., 2007; Poulin et al., 2007). Their role in generating immune responses is currently unclear, and a recent study observed that they were precommitted to inducing immune tolerance (Shklovskaya et al., 2011).

pDCs are broadly distributed throughout the body, found mostly in the blood. They are known for their robust type-I interferon production upon viral infection, which inhibits viral replication and activates the antiviral functions of mDCs, B, T, and NK cells (Garcia-Sastre and Biron, 2006).

Finally, monocytes can differentiate into moDCs in settings of infection, inflammation, or even steady state (León et al., 2007; Varol et al., 2007; Randolph et al., 1999). Thought of as 'inflammatory DCs', these cells may act as emergency DCs by collecting antigen at the site of infection, transporting it to the lymphoid organs, and differentiating into moDCs (Geissmann et al., 2003; Randolph et al., 1999; Serbina and Pamer, 2006). In mice treated with LPS or gram-negative bacteria, these moDCs were, in fact, the predominant APC (Cheong et al., 2010).

1.1.2. DC receptors

DCs recognize pathogens through internal and external receptors. Toll-like receptors (TLRs) are molecular pattern recognition receptors that bind to pathogen-specific motifs. To date, 13 mouse and 10 human TLRs have been discovered. TLRs are expressed by DCs and B cells, as well as monocytes, NK cells, and T cells (at low levels) (Caramalho et al., 2003). TLRs can be expressed intracellularly, such as TLR9, which recognizes unmethylated CpG DNA (a bacterial hallmark) (Hemmi et al., 2000), or on the cell surface, such as TLR5, which recognizes the flagellin of extracellular bacteria (Hayashi et al., 2001). Other TLRs recognize viral or protozoic patterns.

CD40 is a costimulatory receptor expressed by APCs. Ligation of CD40 by CD40L (CD154) induces upregulation of CD80, CD86, and MHC II, and leads to subsequent maturation of DCs. It may also be able to act as an endocytic receptor (Becker et al., 2002; Chen et al., 2006). CD40 stimulation induces IL-12p40 production and a T-helper 1-biased immune response (Soong et al., 1996; Kamanaka et al., 1996; Campbell et al., 1996), which is geared toward viruses, intracellular bacteria, and cancerous cells. In one study, use of agonistic CD40 antibody (anti-CD40) alone as an adjuvant with antigen treatment induced a CD8+ T cell immune response, but the response was only 1% antigen-specific (Ahonen et al., 2004). However, in the same study, use of anti-CD40 with TLR agonists (TLR 2, 3, 4, 6, 7, or 9) plus antigen induced CD8+ T cells that were 25% antigen-specific (Ahonen et al., 2004).

MHC II is expressed by APCs. Activated APCs upregulate MHC II expression, in addition to costimulatory molecules such as CD80 and CD86. In addition to binding its cognate T cell receptor (TCR), ligation of MHC II induces activation of the protein tyrosine kinase Syk in DCs, which is necessary for maturation. Additional downstream targets include phospholipase C-ɣ (PLCɣ), protein kinase C (PKC), Erk, and p38 (Al-Daccak et al., 2004). MHC II can also internalize once expressed on the surface of APCs and swap out antigens in an early endosomal compartment distinct from the lysosomal compartment where loading occurs upon initial folding (Pathak et al., 2001; Sinnathamby and Eisenlohr, 2003). It has been shown that

targeting antigen to MHC II induces increased antibody titers to the antigen *in vitro* and *in vivo* (Hedrick and Schwartz, 1983; Skea and Barber, 1993; Frleta et al., 2001).

DEC205 is an endocytic receptor of the macrophage mannose receptor family. The ligand for DEC205 is unknown, though recent work shows a role for DEC205 in recognition of apoptotic/necrotic cells (Shrimpton et al., 2009). Anti-DEC205 antibodies coupled to antigen induce tolerance when given alone, but in combination with adjuvant (such as anti-CD40 or a TLR ligand), DCs mature and induce CD8 and CD4 T cell immune responses. In the spleen, DEC205 is primarily expressed on CD8α+ DCs. This subset of DCs localizes to the T cell areas of the spleen and seems specialized for presentation on MHC I to CD8 T cells (Hawiger et al., 2001; Bonifaz et al., 2002; Dudziak et al., 2007).

1.1.3. Antigen uptake, processing, and presentation

DCs are able to take up antigen through several pathways. First, there is non-specific fluid phase uptake (macro- or micropinocytosis). In this process small particles from the surrounding environment are taken up by inward-budding vesicles, which then fuse with lysosomes. Here, the particles are broken down; they may subsequently be degraded or diverted into MHC pathways for presentation. DCs are also able to take up antigen through their receptors. These receptors, such C-type lectins and mannose receptor (MR), are specific for certain motifs. They bind carbohydrates of pathogens or self

proteins. They may mediate phagocytosis or endocytosis, and some also serve as activating receptors. Dectin-1 and DEC205 are both C-type lectins; the former binds fungal β-glucans in zymosan and triggers IL-23, TNF, and IL-6 production (Gerosa et al., 2008; Yadav and Schorey, 2006), while the latter is thought to bind fragments from apoptotic cells and induces tolerance to antigen if no concurrent costimulation is given (Shrimpton et al., 2009; Bonifaz et al., 2002; Hawiger et al., 2001). MR has a role in endocytic clearance of certain glycoproteins and has also been used to target antigen to DCs (Burgdorf et al., 2007; Lee et al., 2002; Burgdorf et al., 2008).

Traditionally, antigen processing occurs in the proteasome and loading occurs in the endoplasmic reticulum (ER) for the MHC I pathway. Endogenous antigen is cleaved in the proteasome to produce smaller peptides which can be loaded on the MHC I molecules. The peptides are transported out of the cytosol into the ER by transporter associated protein (TAP). Here, MHC I and its adaptor molecule, β2-microglobulin, are partially folded via a series of chaperone proteins. This partially folded complex interacts with TAP; addition of the antigenic peptide stabilizes the MHC I complex, which allows it to be exported to the cell surface via the Golgi.

The MHC II pathway utilizes endocytic proteases to cleave exogenous antigen into peptides that can be presented on MHC II. MHC II bound to the invariant chain is exported from the ER into late endosomes, where the invariant chain is successively cleaved until it is removed completely and

replaced by an endosomally-produced peptide. This complex is then transported to the cell surface for presentation to CD4+ T cells.

The classical view of antigen presentation was divided into two groups: extracellular antigen was presented on MHC II to CD4+ T cells and intracellular antigen was presented on MHC I to CD8+ T cells. However, this did not account for the need to cross-present antigen to CD8+ T cells from pathogens/tumors that did not infect/affect APCs. Although the mechanism is only beginning to be understood, cross-presentation was first described over 30 years ago by Michael Bevan, who showed cytotoxic CD8 T lymphocytes (CTL) could be stimulated by the presentation of exogenous antigen (Bevan, 1976). Recently, it has been described that uptake of antigen by certain receptors (i.e. DEC205, MR, DCIR-2) targets antigen to the MHC I or MHC II pathway (Bonifaz et al., 2002; Dudziak et al., 2007; Burgdorf et al., 2007). While MR routes soluble antigen to the MHC I pathway, DCIR-2 directs to the MHC II pathway, and DEC205 can initiate antigen into either pathway (Bonifaz et al., 2002; Dudziak et al., 2007; Burgdorf et al., 2007, 2008). In the case of MR, routing to the MHC I pathway was shown to be myeloid differentiation primary response gene 88 (MyD88) dependant (Burgdorf et al., 2008). MyD88 is an adaptor protein used by most TLRs to activate the transcription factor nuclear factor κ-B (NFκ-B). When antigen was taken up and TLR signaling initiated at the same time, TAP was translocated into the early endosomes, where it could re-import antigenic peptides processed by the cytosolic

proteasome back into the early endosomes. This did not happen when endotoxin-free soluble OVA was given to these same cells (Burgdorf et al., 2008).

pDCs may also be specialized to quickly cross-present antigen when they become activated. Upon encounter with virus, human pDCs were able to cross-present viral antigen within 6 hours. This cross-presentation was dependent on cathepsins, endosomal acidification, and intracellular stores of MHC I in the recycling endosomal compartment, but did not require the proteasome, indicating the pDCs were processing the viral antigen in early endosomes and loading it onto MHC I molecules in the recycling endosome, bypassing the classical MHC I pathway (DiPucchio et al., 2008). It has also been shown that mouse pDCs are able to cross-present antigen, though seemingly by a different mechanism. Mouriès et al., showed that splenic pDCs captured exogenous antigen but could only cross-present this antigen when acted on by a virus or TLR7 or TLR9 ligand; antigen processing and presentation then occurred via a TAP-dependant mechanism, with no intracellular stores of MHC I observed (Mouries et al., 2008).

1.2. B cells

B cells display many of the same activating receptors as DCs, such as CD40, TLRs, and Fc receptors. Like DCs, B cells also upregulate certain cell surface receptors upon activation, such as CD80, CD86, and MHC II. They are able to present antigen, and *in vivo* studies have shown a role for this in

generating optimal primary and memory T cell expansion (Ron and Sprent, 1987; Rodríguez-Pinto and Moreno, 2005; Crawford et al., 2006). A role for direct targeting of B cells with vaccines has also been show, in which targeting of multiple TLRs on both B cells and DCs was required to generate antibody responses, as was T cell help (Kasturi et al., 2011).

2. Vaccines

In 1796, Edward Jenner used cowpox as a vaccine against smallpox, based on the observation that milkmaids who got cowpox did not get smallpox. Over the next 200 years, vaccines were developed against some of the world's biggest public health burdens, yet the mechanisms behind the generation of such protective immunity were not understood. It has been only recently that scientists have explored the mechanisms of protective immunity by vaccines, as decades of research have not generated a successful vaccine against such pathogens as human immunodeficiency virus (HIV), tuberculosis, and malaria.

Vaccines fall into two categories, live attenuated and non-living vaccines. As the name suggests, a live attenuated vaccine is an altered form of the pathogen itself, generally with lessened virulence or increased immunogenicity. Live attenuated vaccines mimic the natural immune response one would have if they survived live infection with the pathogen; these vaccines are generally against acute static pathogens, such as smallpox, chicken pox, and yellow fever. Non-living vaccines include subunit

vaccines, toxoid vaccines, carbohydrate vaccines, and conjugate vaccines. These vaccines generally require co-administration with an adjuvant, and protection is not life-long, requiring booster immunizations to maintain protective immunity. Pathogens generally trigger multiple innate sensors, such as TLRs, RIG-I-like helicase receptors (RLRs), and NOD-like receptors (NLRs). TLRs are cell surface or intracellular receptors; as discussed earlier, they are pathogen sensors for conserved motifs found in bacteria, viruses, or fungi. RLRs and NLRs are both cytoplasmic sensors, RLRs for RNA viruses, and NLRs for microbial components. Additionally, several sensors in the NLR family are components of different inflammasomes, molecular complexes responsible for activating inflammatory processes by cleaving pro-forms of the inflammatory cytokines IL-1β and IL-18 (Palm and Medzhitov, 2009). Thus, it makes sense that a live attenuated vaccine may also trigger multiple of these innate receptors or pattern recognition receptors (PRRs), and in fact this has been observed (Pulendran and Ahmed, 2011). Furthermore, PRRs have been observed to have an additive effect (Kasturi et al., 2011), and non-living vaccines may not be inducing adequate activation of these pathways to generate robust, long-lasting immunity.

Many of the current Food and Drug Administration-approved vaccines, such as hepatitis, yellow fever, and diphtheria, generate protective immunity through neutralizing antibody responses. However, recent studies have elucidated roles for T cell immunity as well. Varicella-specific T cells were

found to be correlates of protection for infection (chicken pox) and reactivation (shingles) (Arvin, 2008; Levin et al., 2008), and magnitude of influenza-specific T cells was found to be inversely correlated to protection in the elderly (McElhaney et al., 2006). Furthermore, it is hypothesized that vaccines against tuberculosis and other pathogens will require strong T cell responses to be effective (Hoft, 2008).

2.1. Particle-based vaccines

Delivery of cargo and appropriate signals to relevant cells represents a significant challenge in development of vaccines. Protein antigens may be cleared by the mononuclear phagocytic system, or lead to tolerance if they are given without proper costimulation. Nano- and microparticles can address this issue by packaging antigen, costimulation, and/or targeting into a safe delivery vehicle. These particles may have increased half-life, stability, and delivery to the target cell population than the individual components themselves. In addition, by packaging multiple components into a particle, off-target effects may also be reduced, such as inflammation caused by activation of cells that did not receive antigen. Finally, particles can be formulated in different ways to change size and rate of biodegradation, and they may be modified to encapsulate cargo or present it on the particle surface.

Nano- and microparticles may be targeted to cells by passive or active targeting. Particles are passively targeted based on their physical properties, such as size. A particle that is <5.5nm in diameter is rapidly cleared via the

kidneys (Choi et al., 2007), while particles from 10nm up to several micrometers in diameter have all been used to deliver antigen. For targeting of immune cells, smaller particles are able to target to lymphoid organs, such as spleen and lymph nodes, while larger particles must be taken up by phagocytic cells (such as monocytes and dendritic cells) and carried to the lymphoid organs. In addition, smaller particles may be taken up by phagocytes and non-phagocytes alike, but larger particles, such as the microparticles, may only be taken up by phagocytes. Active targeting is achieved by introduction of a component on the particle that targets its interaction to a specific cell type or organ, such as an antibody that is specific for a cell surface receptor. Receptors to be targeted are generally endocytic and selectively expressed by the cell type desired. Antibodies (or other ligands) may be attached to the particle surface via biotin-streptavidin interactions, thiolation, or cross-linking agents such as Bis(sulfosuccinimidyl)suberate (BS3).

2.1.1. pH-sensitive hydrogel particles

pH-sensitive hydrogel particles have a polymerized acrylamide backbone, and contain an acid-sensitive crosslinker. The acrylamide and acid-sensitive crosslinker are copolymerized in the presence of cargo antigen by an inverse emulsion polymerization technique (Murthy et al., 2003, 2002). They are formulated to degrade into linear polymer chains at acidic pH, via acid-catalyzed hydrolysis of the crosslinker (Murthy et al., 2003). This

degradation results in release of cargo from the particle, and occurs slowly at pH7.4 (24 hr), but rapidly at pH5 (5 min), the pH of early endosomes in a cell. The degradation causes an increase in osmotic pressure, resulting in water flowing across the membrane and 'bursting' the endosome, a mechanism known as colloid osmotic disruption. The 'burst' releases the contents of the endosome into the cytoplasm of the cell, which allows for presentation of the cargo antigen on MHC I to CTLs, key immune responders that can kill infected cells. Colloid osmotic disruption of the endosomes to produce presentation of antigen on MHC class I was first described 30 years ago; researchers provided antigen to be pinocytosed in hypertonic medium, then switched to iso- or hypotonic medium to produce an osmotic lysis of the pinosome (Okada and Rechsteiner, 1982; Moore et al., 1988). Importantly, this technique did not result in cell death, even after multiple treatments. Ordinarily, the particle and its cargo would be shuffled through increasingly acidic endosomes until coming to the lysosome, where it would be degraded; presentation of antigen would be limited or restricted to MHC II. In addition to releasing antigen into the cytoplasm, the 'burst' caused by the particle degradation also seemed to activate APCs. BMDC given non-degradable particles had a stellate (immature) appearance, while BMDC given pH-sensitive degradable particles had a dendritic (mature) appearance (Kwon et al., 2005b).

2.1.2. Luminescent porous silica nanoparticles

Luminescent porous silica nanoparticles (LPSiNPs) are biodegradable, low-toxicity particles with an intrinsic near-infrared photoluminescence. Silicon is a common trace element in humans, and a degradation product of silicon, orthosilicic acid [$Si(OH_4)$], is found in numerous tissues. This degradation product has been shown to be renally cleared by humans (Popplewell et al., 1998). In mice, LPSiNPs have a blood half-life of 27.6 min ± 1.8 min, while coating the surface of the LPSiNPs with dextran increases their half-life to 82 min ± 5.8 min (Park et al., 2009b), possibly by slowing the rate of hydrolysis of SiO_2 on the particle surface. The particles are noticeably cleared from spleen and liver by 1 week, and completely cleared by 4 weeks (Park et al., 2009b). Other nanoparticles require addition of a fluorescent tag to be tracked *in vivo*, but degradation and trafficking of LPSiNPs may be tracked by their intrinsic photoluminescence, which has an emission of 650-900nm. Additionally, these particles are much more photostable than fluorescein, Cy5.5, or Cy7 (Park et al., 2009b), allowing elimination of autofluorescence signal by measuring the signal at a later timepoint, when background signal has dropped.

The structure of LPSiNPs can act as a host matrix for antigens, antibodies, and other cellular ligands. The particle surface of SiO_2 is negatively charged, and certain positively charged entities may bind to the surface via electrostatic forces. Importantly, avidin is one such entity, which allows for particles to be made with biotinylated components or combinations

of biotinylated components, such as antibodies, antigens, and certain TLR ligands. Additionally, this allows for multiple antibodies or ligands to be densely displayed on the particle surface, potentially producing a multivalent effect and engaging multiple receptors per cell.

Chapter II

Antigen-Loaded pH-Sensitive Hydrogel Microparticles are Taken Up by Dendritic Cells with No Requirement for Targeting Antibodies

Abstract

Particle-based delivery of encapsulated antigen has great potential for improving vaccine constructs. In this study, we show that antigen-loaded, pH-sensitive hydrogel microparticles are taken up and presented by bone marrow-derived dendritic cells (BMDCs) in vitro and are targeted to dendritic cells (DCs) and monocytes in vivo. This uptake is irrespective of targeting antibodies. BMDCs in vitro and DCs in vivo also display upregulation of activation markers CD80 and CD86 when treated with microparticles, again with no difference in conjugated antibodies, even agonistic CD40 antibody. We further show that these particles induce enhanced expansion of cytokine-producing CD8 T cells in response to challenge with ovalbumin-expressing vesicular stomatitis virus, in both an accelerated vaccination strategy using pre-loaded BMDCs and a traditional mouse immunization setting.

1. Introduction

Vaccine strategies based on protein antigens are sought-after based on their low toxicity and broad applications (Berzofsky et al., 2001). They show promise in inducing CD4 and CD8 T cell responses, which are required for effective vaccines against certain pathogens and cancers. However, suitable methods of delivery are required for protein antigens, they can be degraded due to their small size or taken up by non-beneficial cell subsets, and proteins presented in the absence of an adjuvant are frequently tolerogenic (Janeway, 1989; Walker and Abbas, 2002). Particles have been made from lipids, proteins, silica, and polymeric systems to enhance delivery of protein antigens (Zhang et al., 2008). Biodegradable polymeric nano- or microparticles, such as poly(lactic-co-glycolic acid) (PLGA) and pH-sensitive hydrogels are particularly attractive delivery vehicles, as they can encapsulate cargo, present targeting moieties on their surface, and are easily formulated to control for their size and intracellular release kinetics (Mundargi et al., 2008; Boyle and Woolfson, 2011).

We have chosen to use pH-sensitive hydrogel particles; these particles are stable at pH7.4, but upon phagocytosis and entry into the endosomes, they degrade into linear polymer chains and small molecules due to incorporation of an acid-sensitive crosslinker in their matrix (Murthy et al., 2003). The proposal is that they produce a colloid osmotic disruption of the endosome, and this releases their cargo into the cytoplasm allowing for

presentation via the MHC class I pathway (Murthy et al., 2003). This lysosomal disruption may activate bone marrow-derived dendritic cells (BMDCs); BMDCs that take up degradable hydrogel nanoparticles display a dendritic (mature) cell surface, while BMDCs that take up non-degradable hydrogel nanoparticles display a stellate (immature) surface (Kwon et al., 2005b). Leakage into the cytoplasm also circumvents possible degradation by hydrolytic enzymes in the late endosomes or lysosomes (Murthy et al., 2003; Standley et al., 2004). Additionally, these particles remain neutral upon degradation, limiting potential toxicity and charge interactions with proteins (Sassi et al., 1996). In contrast, degradation of PLGA produces glycolic and lactic acid, which creates an acidic microenvironment that can denature and inactivate encapsulated proteins (Zhu et al., 2000).

pH-sensitive hydrogel particles have been used to deliver the model antigen ovalbumin (OVA) in several studies. In one study, particles induced cell surface receptors indicative of activation on BMDCs even in the absence of adjuvant (Standley et al., 2007). Particles have been made that incorporate CpG to provide increased activation (Standley et al., 2007; Kwon et al., 2005b), and other particles have incorporated DEC205-specific antibodies via amine groups on the particle surface for targeting to DCs (Kwon et al., 2005a). However, even without activating or targeting components, an OVA-encapsulating particle enhanced survival rates for mice injected with OVA-expressing EG7 tumor cells (Standley et al., 2004). It should be noted that

only phagocytic cells, such as macrophages and dendritic cells, are able to engulf particles ~0.5-3μM in diameter to an appreciable extent; thus, microparticles such as the ones used in the above-mentioned studies are passively targeted to antigen presenting cells (APCs) simply based on their size.

We produced 1.5μM, pH-sensitive hydrogel microparticles encapsulating OVA with various antibodies decorating the surface to determine if targeting and/or activating components could enhance APC-microparticle interactions. We selected a DEC205-specific antibody (anti-DEC205) as the targeting antibody, agonistic CD40 antibody (anti-CD40) as an activating component, and hemagluttinin antibody (anti-HA) as a negative control antibody. DEC205 is an endocytic receptor, thought to be involved in recognizing ligands expressed by apoptotic or necrotic cells and found primarily on $CD8^+$ DCs (Shrimpton et al., 2009). Anti-DEC205 has been conjugated with antigen and utilized to target that antigen to DCs. However, without concomitant delivery of adjuvant, such as anti-CD40, DEC205 targeting induces tolerance to the antigen (Bonifaz et al., 2002). Anti-HA recognizes the nonapeptide sequence YPYDVPDYA derived from the human influenza virus hemagluttinin (HA) protein, and as such, will not react with mouse cells. Thus, we engineered OVA-encapsulating particles displaying anti-DEC205 or anti-HA with or without anti-CD40 to determine if receptor-mediated endocytic targeting is observed with our formulation of particles, and

to determine if anti-CD40 is required for activation or to enhance activation of APCs by the particle. As a control, OVA-encapsulating particles without antibodies were also produced.

2. Materials and Methods

2.1. Mice

OT-I (CD8 TCR transgenic OVA-specific mice), OT-II (CD4 TCR transgenic OVA-specific mice), and C57BL/6 mice were purchased from the Jackson Laboratories and maintained in specific pathogen-free facilities at UCSD. Animal protocols were approved by the Institutional Animal Care and Use Committee.

2.2. Antibody preparation

Anti-HA (12CA5), anti-DEC205 (NLDC-145), and anti-CD40 (FGK45.5) hybridomas were obtained from American Type Culture Collection. Antibodies were then produced by BioNexus**,** purified using Montage Prosep G kit (Millipore), and used in production of microparticles.

2.3. Preparation of microparticles

Reverse emulsion polymerization technique was used to encapsulate OVA into acid-sensitive hydrogel microparticles. After formulation, Bis(Sulfosuccinimidyl)suberate (BS3) was used to conjugate the antibodies to

the particles' surface. Experimental details are described in the supplementary material.

2.4. Antibody conjugation efficiency and binding activity

The conjugation efficiency was measured by comparing the initial antibody concentration to the concentration of unbound antibodies after the conjugation reaction. The antibody samples were boiled for 5 min in 1x SDS loading buffer (Bio-Rad) and loaded on a 10% SDS poly-acrylamide gel (Bio-Rad). The gel was stained with Coomassie blue (Bio-Rad) for 3 hours followed by 3 destaining washes.

The binding activity of anti-HA-conjugated particles encapsulating OVA (MP HA) was compared to particles without antibody encapsulating OVA (MP). A sample of particles containing 15µg of MP HA or MP was mixed with 3-fold dilutions of fluorescein-labeled HA peptide [YPYDVPDYA; highest dose: 1170ng (900pmol); Synthetic Biomolecules]. Unbound peptide was washed away using BioSpin Columns (Bio-Rad) and the bound HA peptide on particles was measured for fluorescence intensity.

2.5. BMDC cultures

BMDCs were prepared as described (Dejean et al., 2009) and harvested on day 8.

2.6. T cell isolation and purification

For T cell purification, spleens and lymph nodes (LNs) were taken from OT-I or OT-II mice. Red blood cell (RBC) lysis of splenocytes was done using ACK lysis buffer (0.15M NH_4Cl, 1M $KHCO_3$, 0.1mM Na_2EDTA). Cells were then incubated with a mixture of biotinylated anti-B220 (RA3-6B2, eBioscience—all antibodies are from eBioscience unless otherwise noted), anti-Gr-1 (RB6-8C5), anti-MHC class II (M5/114.15.2), anti-DX5 (DX5), anti-CD11b (M1/70), anti-Ter119 (TER119), and either anti-CD4 (OT-I purification; GK1.5) or anti-CD8α (OT-II purification; 53-6.7). LNs were incubated with a mixture of biotinylated anti-B220 and anti-CD4 (OT-I purification) or biotinylated anti-B220 and anti-CD8α (OT-II purification). Cells were then negatively selected with streptavidin-coupled microbeads (Miltenyi Biotec).

2.7. ^{3}[H]-thymidine proliferation assay

20,000 BMDCs were cultured for 1 day at 37ºC with 3-fold dilutions of microparticles or EndoGrade OVA (highest dose 1µg/mL), then washed twice and incubated with 150,000-200,000 magnetic bead-sorted OT-I or OT-II T cells for 3 days at 37ºC. 1µCi/well ^{3}[H]-thymidine (Perkin Elmer Life Sciences) was added for the last 8 hours of culture.

2.8. In vitro activation

BMDCs were cultured for 2 days at 37ºC with 3-fold dilutions of microparticles or EndoGrade OVA (highest dose 1μg/mL). 10μg/mL lipopolysaccharide (LPS, Sigma) and PBS were used as controls. Cells were resuspended in FACS buffer (PBS with 1mM EDTA, 1% FCS, and 0.1% sodium azide), incubated with anti-mouse FcγRII-III (supernatant from hybridoma 2.4G2 cultures) for 15 min at 4ºC, and stained with anti-CD80 FITC (16-10A1, Biolegend), anti-CD86 PE (GL1), anti-B220 PerCP (Biolegend), and anti-CD11c Allophycocyanin (N418) for 20 min at 4ºC.

2.9. In vivo DC activation and fluorescent particle uptake

10μg microparticles were injected subcutaneously (s.c.) in both hind footpads of mice (20μg/mouse, 3-4 mice/group). Mice were sacrificed at day 1 for fluorescent particle uptake and day 2 for *in vivo* DC activation. Popliteal and inguinal LNs were taken and analyzed by flow cytometry.

2.10. BMDC vaccinations for VSV-OVA challenge

BMDCs were incubated overnight with 0.85μg/mL MP HA, 0.85μg/mL MP HA + 0.42μg/mL LPS, 0.42μg/mL LPS + 5μM SIINFEKL peptide (OT-I peptide; derived from OVA257-264, the epitope which CD8 TCR transgenic OT-I mice are specific for; Genemed Synthesis) or PBS control. 250,000 of these BMDCs were injected intravenously (i.v.) into mice (4 mice/group). One

week after BMDC vaccination, mice were challenged i.v. with $1x10^5$ PFU vesicular stomatitis virus-OVA (VSV-OVA; Dr. Leo Lefrançois, University of Connecticut Health Center).

2.11. Vaccination for VSV-OVA challenge

10μg MP HA, 10μg MP HA + 10μg LPS, 10μg LPS + 10μg EndoGrade OVA, 10μg EndoGrade OVA, or PBS were injected s.c. in both hind footpads of mice (4 mice/group). 45 days after vaccination, mice were challenged i.v. with 10^5 PFU VSV-OVA.

2.12. Flow cytometry

PBL, LNs, or spleen were isolated from mice at various time points. For DC analysis, LNs were first incubated for 20 min at 37ºC with collagenase D (1mg/mL; Roche). Single-cell suspensions were prepared and cells from PBL and spleen were subjected to RBC lysis using ACK. Cell staining was performed as BMDC staining above. Antibodies used for: *in vivo* DC activation—CD80 FITC, CD86 PE, CD11c PE-Cy7, B220 APC-Cy7, and CD3 PerCP-Cy5.5 (145-2C11); *in vivo* fluorescent microparticle uptake—Ly6G PE (1A8, BD Pharmingen), B220 APC-Cy7, TCRβ APC-Cy7 (H57-597), Ly6C Allophycocyanin (HK1.4), CD11c PE-Cy7, CD11b eFluor450, CD8 PerCP (Biolegend), CD4 biotin, and streptavidin Qdot525 (Invitrogen); and VSV-OVA challenge experiments—B220 FITC, CD11b FITC, Ter119 FITC (used in

BMDC accelerated vaccination experiment only), CD4 PE-Cy7, CD8 Pacific Blue (Biolegend), and CD44 APC-Cy7 (IM7).

2.13. Intracellular cytokine staining

For detection of intracellular cytokines, PBL, LNs, or spleen were isolated and cultured with 5μM OT-I peptide. After 1 hour, Brefeldin A (1μg/mL; BD Biosciences) was added and the cultures were incubated at 37ºC overnight. Cells were stained as above, then fixed and permeabilized to detect intracellular IFNɣ allophycocyanin (XMG1.2).

3. Results

3.1. Production of pH-sensitive hydrogel microparticles

To produce pH-sensitive hydrogel microparticles, an acid-sensitive crosslinker (Fig 1A) was produced as described (Paramonov et al., 2008; Jain et al., 2007) and copolymerized with acrylamide by inverse emulsion polymerization (Fig 1B). This crosslinker is cleaved by acid-catalyzed hydrolysis; thus, once a particle is taken up, the acidic environment of the endosome will initiate particle degradation and release of its contents, resulting in release of antigen into the cytoplasm. Presumably some endocytic vesicles are shunted into the MHC class II presentation pathway, whereas, access to the cytoplasm also promotes presentation in association with MHC class I (Fig 1B). We chose ovalbumin (OVA) as the cargo to load in the

particles, since the experimental tools for studying the immune response to OVA are extensive. Specifically, to study T cell responses, we used CD8 and CD4 OVA-specific TCR transgenic mice (OT-I and OT-II, respectively) and VSV-OVA, a pathogen engineered to express OVA. The amount of OVA loaded was 2.4μg per mg of particle, with an encapsulation efficiency of 52.6% ±14.7%. We list particle concentration as the amount of OVA in the particle and not the dosage of particle. Following particle formulation, anti-DEC205, anti-HA, and/or anti-CD40 were added via BS3 ligation of amine groups on the antibodies (MP DEC, MP HA, MP CD40, MP DEC CD40, and MP HA CD40; particles without antibodies are referred to as MP). To estimate conjugation efficiency of the antibodies, a protein gel was run comparing total antibody loaded and unbound antibody following BS3 conjugation (Fig 1C). Approximately 75% of antibody starting material was conjugated to the particle, with only minimal non-specific binding. Finally, the particle's average diameter based on volume was 1.5±0.8μM; the measurement was done by laser diffraction particle sizing using a Mastersizer 2000 instrument (Malvern), and confirmed using Multisizer 4 (Beckman) and Qnano (Izone).

3.2. Antibody binding is preserved following production of microparticles

Antibody activity following conjugation to particles is generally not assessed, even though a particle formulation that destroys antibody activity or blocks antibody binding sites effectively nullifies addition of that component.

We developed an assay utilizing fluorescein-tagged HA peptide to determine whether the binding ability of anti-HA was still active following BS3 conjugation. MP HA and MP were incubated with increasing amounts of the labeled HA peptide, excess peptide was washed out, and fluorescence intensity was measured and compared between microparticles (Fig 1D). Greater than 5-fold binding activity was observed for MP HA versus MP, indicating that anti-HA is still capable of binding peptide.

3.3. CD8 and CD4 T cells incorporate ^{3}[H] in an in vitro proliferation assay in the presence or absence of targeting antibodies on microparticles

To determine whether targeting antibodies could influence antigen delivery to DCs and subsequent proliferation by T cells, we incubated microparticles with BMDCs. Following overnight incubation, BMDCs were washed to remove free microparticles and incubated with magnetic-bead sorted OT-I (CD8) and OT-II (CD4) T cells for three days. ^{3}[H]-thymidine uptake was used to quantitate DNA synthesis induced in culture. We found that OVA was presented by BMDCs on both MHC class I and II (Fig 2A) for all microparticles, regardless of conjugated antibodies, whereas, at the concentrations tested, free OVA was ineffective. ^{3}[H]-thymidine incorporation was statistically significant for all microparticles by two-way ANOVA, compared to OVA alone. Fig 2B shows post-hoc testing at the 1μg/mL OVA dose.

3.4. Microparticles induce upregulation of activation markers on DCs in vitro and in vivo

To examine whether microparticles could activate DCs *in vitro*, we incubated BMDCs with the different microparticles for two days, then performed FACS analysis for upregulation of the activation markers CD80 and CD86. All particles similarly induced both molecules, compared with the same dose of OVA (Fig 3A-C). All microparticles conjugated with anti-CD40 upregulated CD80 and CD86 to the same levels as MP DEC, MP HA, or MP, despite the later three not having an activating moiety.

To measure *in vivo* activation of DCs, we injected microparticles s.c. into both hind footpads of mice. Two days later, the mice were sacrificed and popliteal (draining) and inguinal LNs were taken and stained for CD80 and CD86. The microparticles induced modest upregulation of both markers in popliteal LNs (Fig 3D), and CD86 was upregulated in inguinal LNs (Fig 3E). This induction was intermediate compared to LPS activation.

3.5. Fluorescent microparticles interact with monocytes and DCs in vivo

To determine which cells were interacting with (and potentially taking up) microparticles *in vivo*, we made MP, MP HA, and MP DEC using Alexa Fluor 488-tagged OVA. We injected the microparticles s.c. in both hind footpads. Free OVA-Alexa Fluor 488 and PBS were used as controls. Mice were sacrificed 1 day later and popliteal LNs were examined. Cells were

phenotyped as T cells ($TCR\beta^+$), B cells ($B220^+$), plasmacytoid DCs (pDCs, $CD11c^+B220^+$), DCs ($CD11c^+B220^-$), monocytes ($CD11b^{hi}$ $Ly6C^+Ly6G^-$), and neutrophils ($CD11b^{hi}$ $Ly6C^+Ly6G^+$). Interestingly, a substantial $CD11b^{hi}$ $CD11c^{lo}$ population emerged in all microparticle-injected mice that was almost completely absent from OVA-injected or PBS-injected mice (Fig 4A-B). This population consisted of both monocytes and neutrophils, based on Ly6G and Ly6C expression (Fig 4A, bottom row). The percentage of each cell subset (B, T, monocyte, neutrophil, DC, and pDC) present in the popliteal LNs is shown in Fig 4B. Monocyte and neutrophil cell subsets were dramatically increased in these LNs for all microparticle-injected mice versus OVA-injected mice. No increase was observed for the other four subsets.

Popliteal LN cells were analyzed for Alexa Fluor 488 staining to identify the populations that had taken up the microparticles. Monocytes and DCs were most effective at taking up antigen in microparticle-injected mice, while neutrophils were comparatively less efficient (Fig 4C). There was no difference in the efficiency of microparticle uptake compared with OVA in the monocyte and DC subsets, however, as there were many more monocytes in the popliteal LNs of the microparticle-injected mice there was a much larger total number of Alexa Fluor 488+ monocytes in these groups. DC uptake of particles versus OVA was not significantly different (Fig 4C), and no difference was seen in uptake amongst DC subsets ($CD4^+$, CD8+, CD4-CD8- or

DEC205+; data not shown). Finally, no differences in uptake were observed between the different microparticles (Fig 4C).

3.6. VSV-OVA challenge following vaccinations produces increased IFNɣ+ CD8 T cells

To assess memory-inducing potential of the microparticles, two vaccination strategies were used: accelerated vaccination using BMDCs pre-incubated with microparticles, and injection of mice directly with microparticles. As no differences had been observed between the particles in the previous experiments, only MP HA was selected for these experiments.

For accelerated vaccination using BMDCs, we incubated cells with MP HA, MP HA+LPS, PBS, or LPS plus the 8-amino acid antigenic peptide (SIINFEKL) peptide overnight. Cells were then collected and washed, and 250,000 were injected per mouse i.v. (4 mice/group). After 1 week, mice were challenged with VSV-OVA. Mice were bled over the following 2 months and sacrificed at day 55, when spleens were taken. To track immune response to OVA, PBL or spleen cells were restimulated overnight with SIINFEKL in the presence of Brefeldin A, and then analyzed for intracellular IFNɣ. Mice given MP HA or MP HA+LPS BMDCs had a large percentage of IFNɣ+ CD8 T cells (15-20% out of CD8+), as tracked in blood at the peak of the response (Fig 5A). This response was significantly greater than that of the PBS control group. MP HA+LPS was also significantly greater than LPS+OT-I peptide and

MP HA. At sacrifice, spleens from the MP HA+LPS group had a significantly greater percentage of IFNɣ+ CD8 T cells than PBS; LPS+peptide and MP HA groups were also elevated, though not statistically significant (Fig 5B).

The direct immunogenicity of microparticles was also tested. Mice were given MP HA, MP HA+LPS, LPS+OVA, OVA, or PBS s.c. in both hind footpads, and at day 45 they were challenged with VSV-OVA. Immune responses were then tracked in blood, as for the BMDC accelerated vaccination (Fig 5C). At day 17, mice were sacrificed and spleens and LNs were taken. Immune responses of MP HA- and MP HA+LPS-injected mice were similar to the LPS+OVA-injected mice (a secondary immune response to the challenge), while OVA-injected mice displayed an immune response similar to PBS (a primary immune response). No additive effect was observed for MP HA+LPS compared to MP HA. IFNɣ+ CD8 responses in spleen and LNs were elevated in MP HA and MP HA+LPS to similar levels as LPS+OVA (Fig 5D-E).

4. Discussion

We have produced 1.5μM, OVA-encapsulated, pH-sensitive hydrogel microparticles, with or without targeting and activating antibodies. These particles were all effective at generating CD4 and CD8 T cell responses *in vitro* and activating DCs *in vitro* and *in vivo*. No preferential uptake was observed with MP DEC versus MP HA. No increased activation was observed with microparticles displaying an antibody that binds CD40 and stimulates an

activation program in DCs and B cells (Rolink et al., 1996). Testing of MP HA construct revealed that antibody binding sites were still active, indicating that particle production did not damage the antibodies. MP HA immunization and BMDC-MP HA transfer both showed an expanded CD8 T cell response to VSV-OVA challenge, more comparable to a secondary than a primary immune response.

Interestingly, *in vivo* uptake of our microparticles is dominated by monocytes. DCs also take up the particles, though at the same level as fluorescent OVA. Monocytes and neutrophils are both recruited to the draining LN in large numbers, with ~10-fold more monocytes and ~40-50-fold more neutrophils in microparticle-injected versus OVA-injected counterparts. However, monocytes are the primary cell type that interacts with the particles; in the draining LN, mice immunized with any of the microparticles have ~10-fold more particle-positive monocytes compared to OVA^+ monocytes in mice immunized with OVA. Monocytes can differentiate into monocyte-derived DCs (moDCs) in cases of inflammation, infection, or even at steady state (Randolph et al., 1999; León et al., 2007; Varol et al., 2007). We hypothesize that monocytes may pick up the particle in the footpad and then move to the draining LN, where they may further differentiate into these APCs. In fact, fluorescent microspheres 0.5-1μM in size injected s.c. have demonstrated this same occurrence (Randolph et al., 1999). Additionally, it has been shown recently that in mice treated with LPS or gram-negative bacteria, peripheral

monocytes migrate to LNs, differentiate into moDCs, and become the predominant APC (Cheong et al., 2010). The large neutrophil recruitment we observe may be due to their phagocytic nature, an acute inflammation occurring in response to the particles, or perhaps even to modulate the DC or moDC response. While neutrophils are typically thought of as short-lived cells that are recruited to phagocytose cells and release effector molecules, they have also been shown to compete for antigen in the LN (Yang et al., 2010) and induce maturation of DCs or moDCs (van Gisbergen et al., 2005b; a; Megiovanni et al., 2006; Bennouna and Denkers, 2005).

The results illustrate a pathway to improved vaccination by focusing on the facilitated uptake of microparticles and on their ability to induce DC and myeloid activation.

Acknowledgements

We acknowledge Osayi Eidgin and Jamie Moser for their help in preparing the hydrogel particles. L.E.R. was supported by University of California, San Diego (UCSD) Immunology training grant NIH T32AI060536. J.M.M. was supported by UCSD IRACDA Fellowship Grant GM06852. We thank NIH Directors New Innovator Award (1 DP2 OD006499-01) and King Abdul Aziz City of Science and Technology (KACST) for financially supporting this study.

Contributions

L.E.R., E.A.M., J.M.M., J.S., A.A., M.C., and S.M.H conceived and designed the research. L.E.R., E.A.M., J.M.M., J.S., and C.D.K performed the experiments. L.E.R., E.A.M., A.A., J.M.M., and J.S. analyzed the data. L.E.R., E.A.M., J.M.M., J.S., A.A., M.C., and S.M.H. wrote the manuscript.

Competing Interests Statement

The authors declare no competing financial interests.

Figures

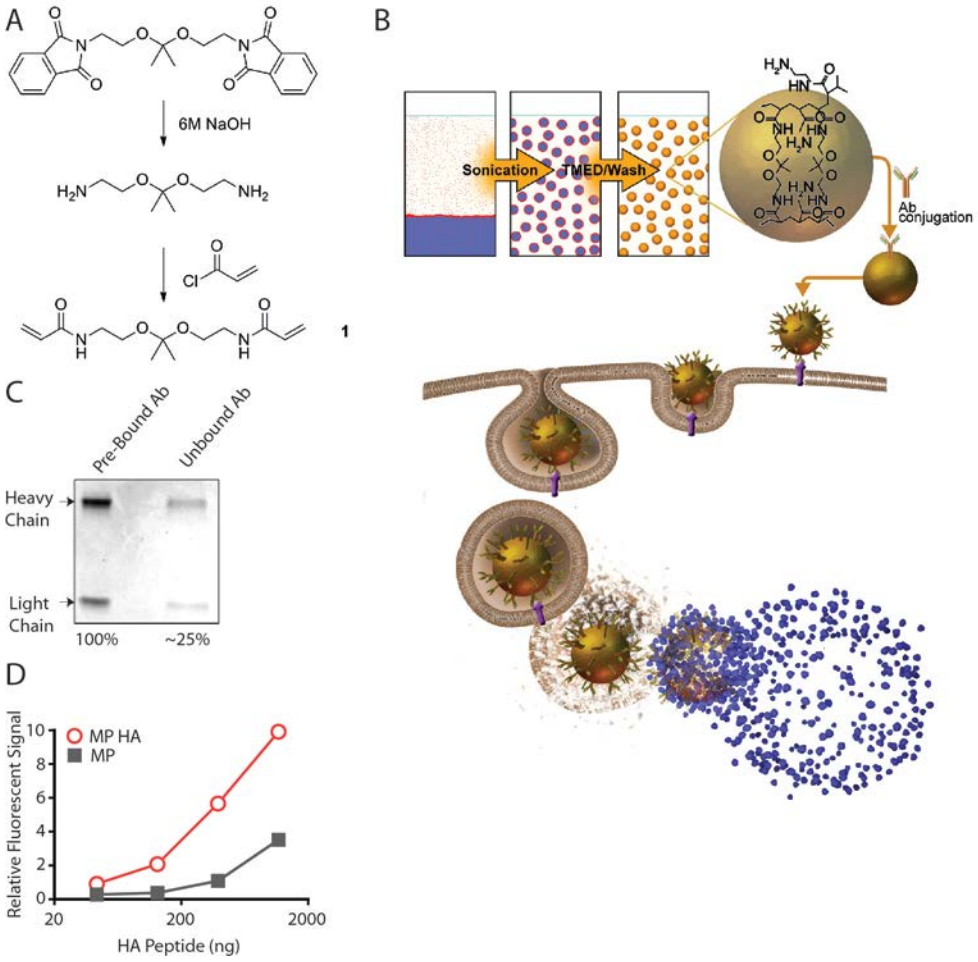

Figure 1. Antibodies can be conjugated to pH-sensitive hydrogel microparticles and maintain binding activity. A) Synthesis of acid-sensitive crosslinker. **B)** Schematic of microparticle production, uptake by a cell, and release of cargo in the endosome. **C)** Conjugation efficiency of antibodies to particles. **D)** Fluorescein-HA peptide binding activity of MP HA compared to MP.

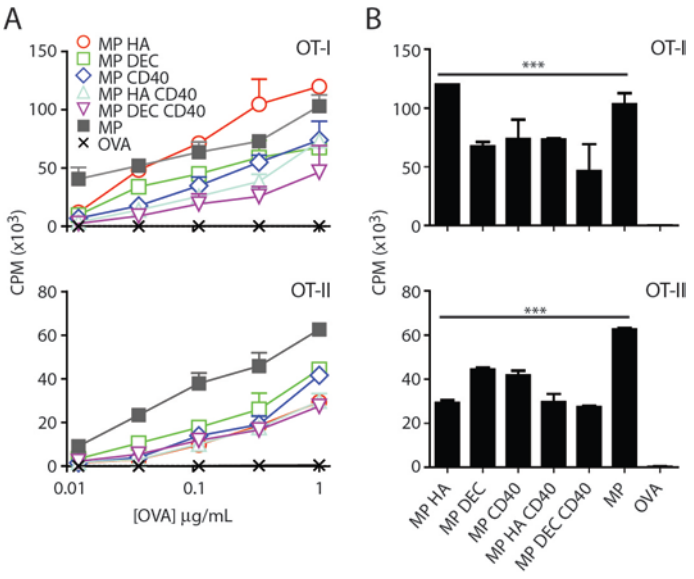

Figure 2. Co-culture with microparticle-injected BMDCs produced CD8 and CD4 proliferation *in vitro*. BMDCs were incubated with 3-fold dilutions of microparticles or OVA (highest dose: 1µg/mL) for 1 day. Cells were then incubated with OT-I (CD8) or OT-II (CD4) T cells for 3 days. 1µCi/well ^{3}[H]-thymidine was added for the final 8 hours of culture. **A)** Graph of CPM vs dose (amount of OVA in microparticles). Data shown are mean+SD. Two-way ANOVA was ***p<0.001 for OT-I and OT-II. **B)** CPM graphs for microparticles at 1µg/mL OVA with two-way ANOVA Dunnett's post-hoc test. Microparticles are compared to OVA. ***p<0.001

Figure 3. All microparticles, regardless of antibody conjugation, induce upregulation of CD80 and CD86 on BMDCs. BMDCs were incubated with 3-fold dilutions of microparticles or OVA (highest dose: 1μg/mL). Controls were PBS or LPS. After 2 days, cells were stained with CD80, CD86, B220 and CD11c and analyzed by flow cytometry. **A)** Graphs are MFI of CD80 or CD86 for CD11c+B220- cells. Two-way ANOVA for CD80 and CD86 *** $p<0.001$. **B)** CD80 and CD86 graphs for microparticles at 1μg/mL OVA with two-way ANOVA Dunnett's post-hoc test versus OVA. PBS and LPS were not included in ANOVA analysis. **C)** Representative histograms of CD80 and CD86 staining. Shown: OVA, MP HA, both 1μg/mL OVA, and PBS. **Microparticles induce intermediate activation of DCs *in vivo*.** Mice were given 10μg microparticles s.c. in both hind footpads. After 2 days, mice were sacrificed and popliteal and inguinal LNs were taken. Cells were stained for CD11c, B220, CD3, CD80, and CD86. Graphs are MFI of **D)** CD86 or **E)** CD80 for CD3-B220-CD11c+ cells. 4 mice/group. Statistics are one-way ANOVA with Dunnett's post-hoc test (compared to OVA). *$p<0.05$, **$p<0.01$, ***$p<0.001$

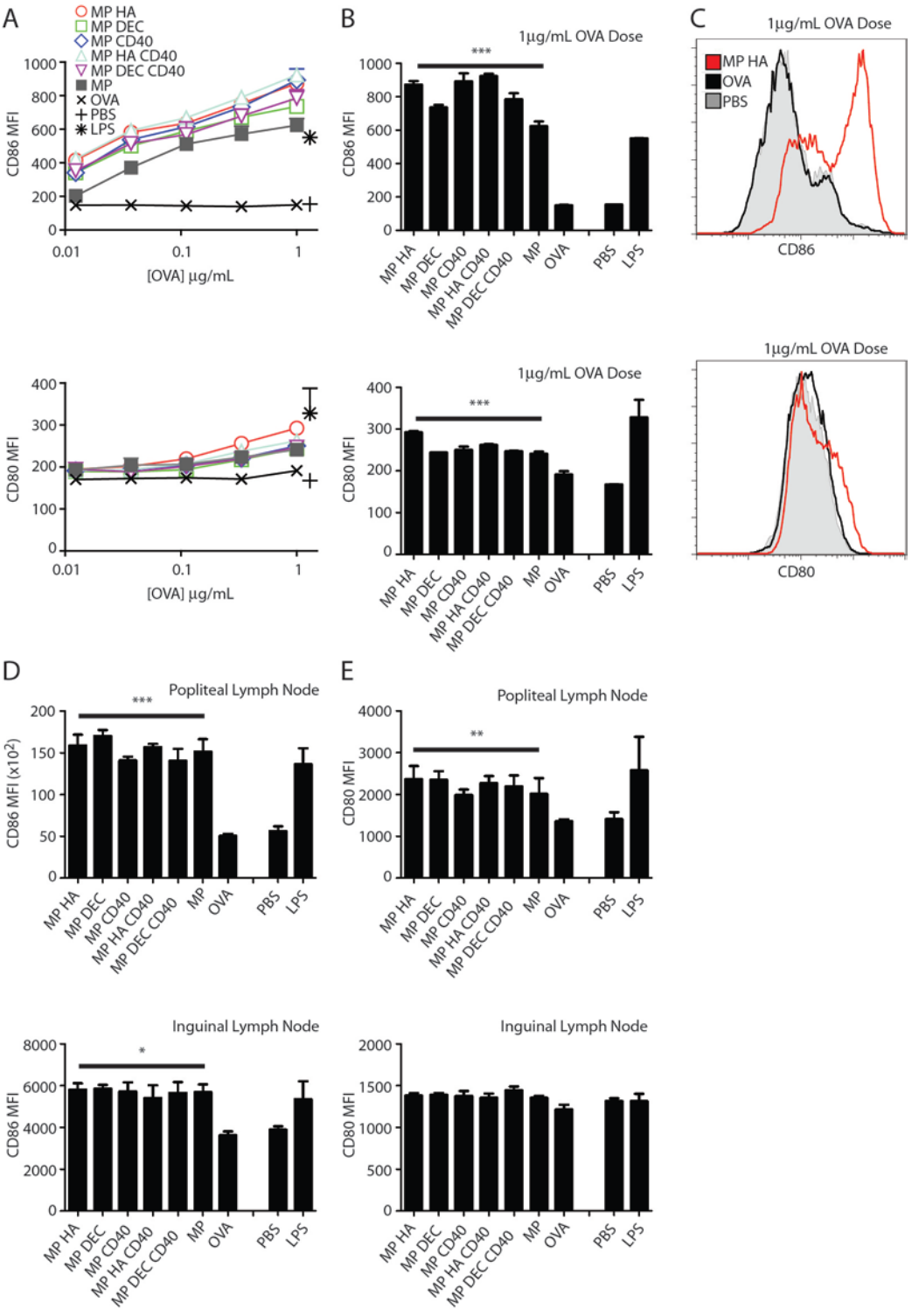
A
MP HA
MP DEC
MP CD40
MP HA CD40
MP DEC CD40
MP
OVA
PBS
LPS
CD86 MFI
[OVA] µg/mL
B
1µg/mL OVA Dose
***
CD86 MFI
MP HA
MP DEC
MP CD40
MP HA CD40
MP DEC CD40
MP
OVA
PBS
LPS
C
1µg/mL OVA Dose
MP HA
OVA
PBS
CD86
CD80 MFI
[OVA] µg/mL
1µg/mL OVA Dose
***
CD80 MFI
CD80
D
Popliteal Lymph Node
***
CD86 MFI (x10²)
Inguinal Lymph Node
*
CD86 MFI
E
Popliteal Lymph Node
**
CD80 MFI
Inguinal Lymph Node
CD80 MFI

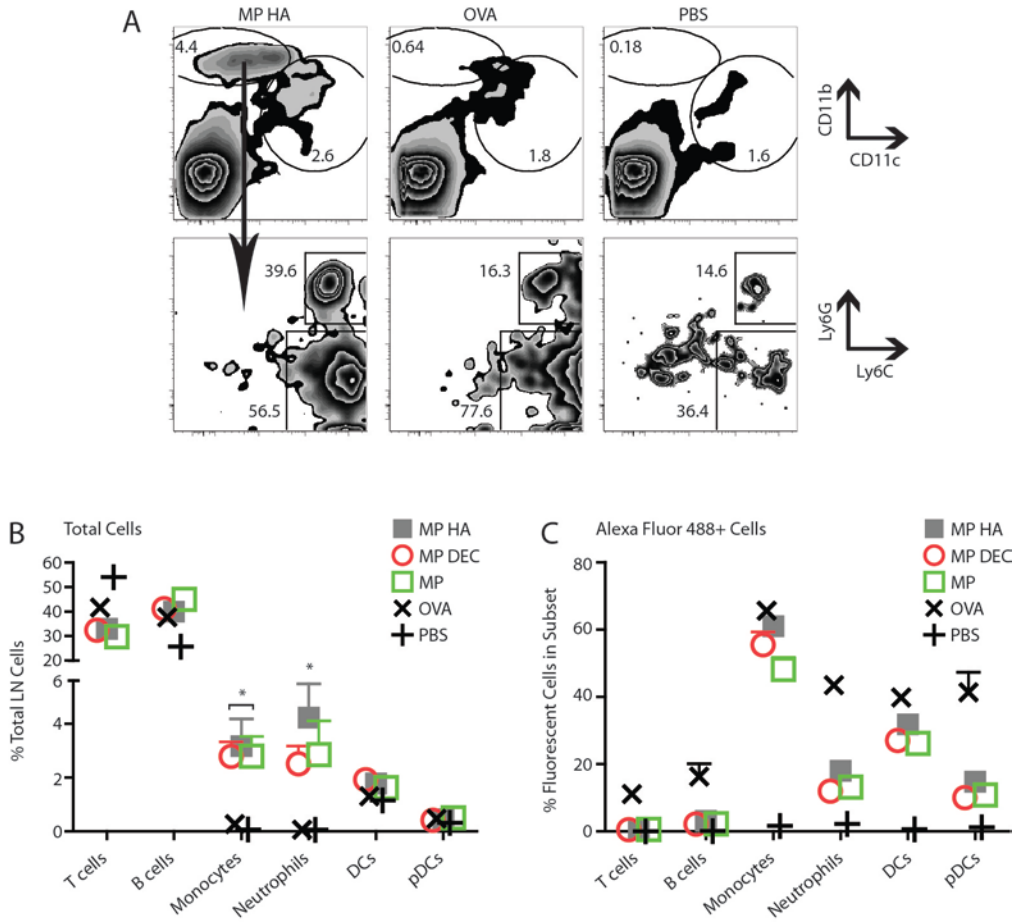

Figure 4. Fluorescent particles recruit neutrophils and monocytes to the draining LN. 10µg microparticles encapsulating OVA Alexa Fluor 488 were injected s.c. in both hind footpads. Mice were sacrificed after 1 day, and popliteal LNs were taken. Cells were stained for CD11c, CD11b, B220, TCRβ, CD4, CD8, Ly6G and Ly6C. **A-B.** Graphs shown were previously gated on live cells (FSC vs SSC). **A)** All microparticle groups caused a large recruitment of $CD11b^{hi}$ $CD11c^{lo}$ cells that was not observed in OVA- or PBS-injected mice. Shown are representative FACS plots from MP HA-, OVA-, and PBS-injected mice. **B)** $CD11b^{hi}$ $CD11c^{lo}$ cells were both neutrophils and monocytes. **C-D.** Data was combined from two experiments, three mice each. **C)** The percentage of monocytes and neutrophils was increased in microparticle- versus OVA-injected popliteal LNs. **D)** The efficiency of particle or OVA uptake for each cell subset.

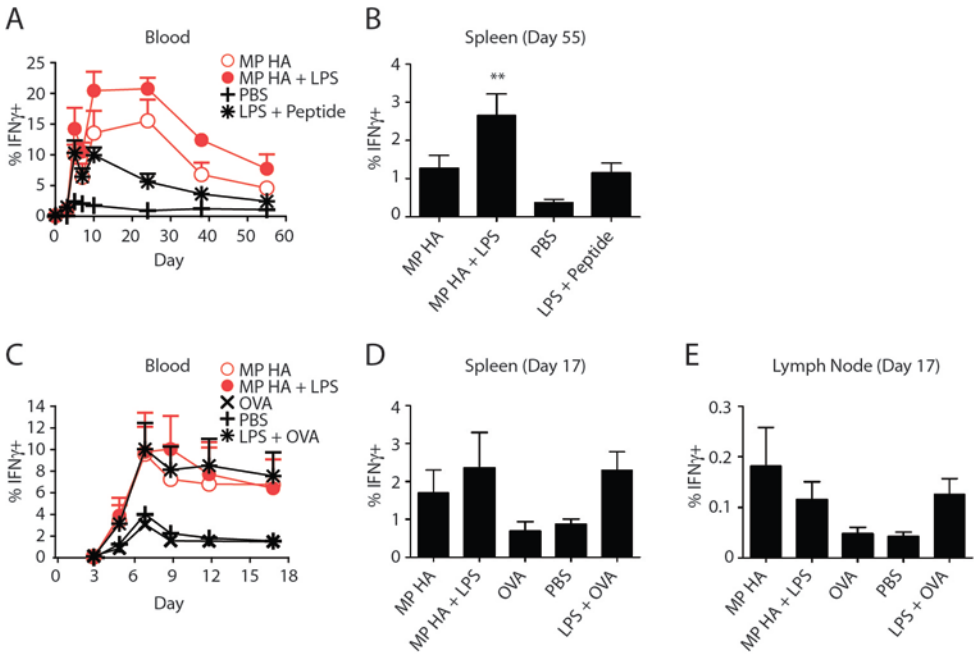

Figure 5. Secondary immune response to VSV-OVA challenge. A-B. BMDCs were incubated overnight with 0.85μg/mL MP HA, 0.85μg/mL MP HA + 0.42μg/mL LPS, 0.42μg/mL LPS + 5μM SIINFEKL (OT-I peptide), or PBS control. 250,000 of these BMDCs were given to mice i.v. 7 days post-BMDC injection, mice were challenged with 10^5 PFU VSV-OVA i.v. and **A)** the T cell response was tracked via blood on days 0, 3, 5, 7, 10, 24, 38, and 55 post-challenge. Lymphocytes from blood were purified, restimulated with OT-I peptide, and stained for CD4, CD8, IFNɣ, CD44, B220, Ter119, and CD11b. Antigen-specific cells were detected by IFNɣ+CD44+ staining. Data shown is previously gated on CD8+ T cells. **B)** At day 55, mice were sacrificed, spleens were taken, and antigen-specific cells were detected as in blood. One-way ANOVA was done with Bonferroni post-hoc testing. **C-D. Microparticle vaccination and VSV-OVA challenge.** Mice were given 10μg MP HA, 10μg MP HA + 10μg LPS, 10μg LPS + 10μg EndoGrade OVA, 10μg EndoGrade OVA, or PBS s.c. in both hind footpads. At day 45, mice were challenged with 10^5 PFU VSV-OVA i.v., **C)** and subsequently bled at days 3, 5, 7, 9, 12, and 17. Lymphocytes from blood were purified, restimulated with OT-I peptide and stained for CD4, CD8, IFNɣ, CD44, B220, and CD11b. Antigen-specific cells were detected by IFNɣ+CD44+ staining. Data shown is previously gated on CD8+ T cells. **D)** At day 17, mice were sacrificed, spleens and LNs were taken, and antigen-specific cells were detected as in blood.

Supplementary Information:

5. Supplemental Methods

5.1. Preparation of microparticles

5.1.1. Materials

EndoGrade OVA (Biovendor)

N-(3-Aminopropyl) methacrylamide-HCl (Polysciences)

Acrylamide, ammonium persulfate (APS), Span 80, Tween 80, N,N,N,',N' Tetramethylethylenediamine (TMED), and Docusate sodium salt (AOT, Sigma)

Mannitol (Pearlitol 25C, Roquette, France)

OVA Alexa Fluor 488 (Invitrogen)

Bis(Sulfosuccinimidyl)suberate (BS3, Thermoscientific)

5.1.2. Preparation of acid sensitive crosslinker

Synthesis of the acid-sensitive crosslinker **(1)** is depicted in Fig 1A and described in ref (Jain et al., 2007; Paramonov et al., 2008). ^{1}H NMR is shown in Fig 6.

5.1.3. Formulation of hydrogel microparticles

Ovalbumin (1mg) was dissolved into 250µl 10mM Tris-HCl buffer, pH 8, followed by the addition of acrylamide (61.3mg, 862.4µmol), N-(3-

Aminopropyl) methacrylamide-HCl (1.3mg, 9.15μmol), acid-sensitive crosslinker (12.4mg, 45.9μmol) and APS (8mg, 35μmol). To produce an emulsion, 2.5mL 3% 3:1 Span 80:Tween 80 in hexanes were added to the aqueous phase followed by 30 seconds of sonication at an amplitude of 40 (1/8" tip, Misonix 4000s). The polymerization was initiated by the addition of 25μl TMED and the particles were left to stir for 10 min at room temperature (R.T.). The particles were collected by centrifugation at 4,000xg for 5 min and washed with hexanes (10mL, two times) then with acetone (10mL, three times), and then in PBS, pH 8. The particles were dispersed in PBS, pH 8, passed through a 30μm filter, and lyophilized after the addition of 5% mannitol. OVA Alexa Fluor 488 was used to prepare particles used for in vivo uptake studies.

5.1.4. Encapsulation efficiency

The encapsulated OVA was released from the particles by acidifying the solution with 0.1N HCl to dissolve the particles followed by neutralization with 0.1N NaOH. The amount of OVA was determined using the BCA assay (Pierce) and compared to that of OVA dilutions treated the same as that of the particles. Encapsulation efficiency of OVA was 52.6% ±14.7%.

Amounts of microparticles are listed as the absolute amount of encapsulated OVA (μg) or as OVA concentrations in a certain volume (μg/ml). Encapsulated OVA was determined to be 2.4μg OVA/mg particle powder.

5.1.5. Particle conjugation to antibodies

To allow BS3 to react with the amine group in N-(3-Aminopropyl) methacrylamide-HCl, microparticle powder corresponding to 0.5mg OVA was resuspended in 1mL PBS pH 8, 1mg BS3 was added (1.7μmol), and the mixture was shaken at R.T. for 30 min. The free BS3 was removed by centrifuging the particles at 12,100xg for 30 seconds and washing with PBS, pH 8. Then, antibody solution corresponding to 0.1mg (0.1mg for one antibody, or 0.1mg each for two antibodies) was added and the microparticles were mixed by placing on the shaker at R.T. for another 30 min. Unbound antibody was separated by washing the particles, centrifugation, and resuspension in 10mM Tris-HCl, pH 8. Finally, the particles were lyophilized in the presence of 5% mannitol.

Supplemental Figure

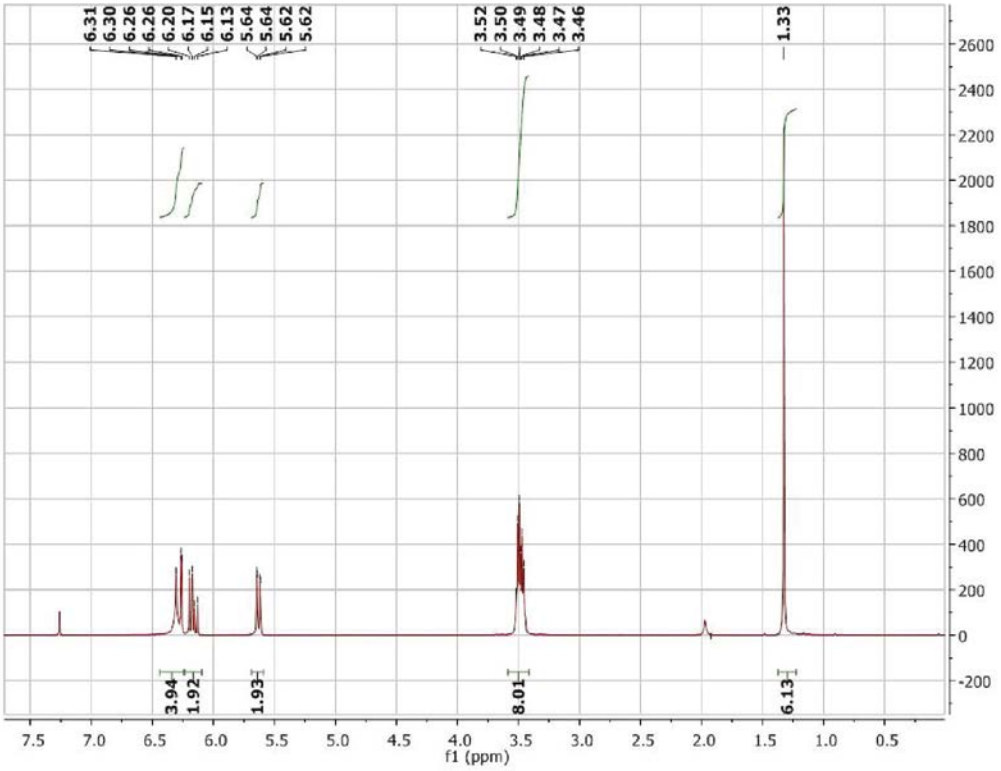

Figure 6. ^{1}H NMR of acid-sensitive crosslinker. ^{1}H NMR (400 MHz, CDCl3) δ 6.28 (dd, J = 17.0, 1.6 Hz, 4H), 6.16 (dd, J = 17.0, 10.1 Hz, 2H), 5.63 (dd, J = 10.1, 1.6 Hz, 2H), 3.49 (dt, J = 14.4, 5.1 Hz, 8H), 1.33 (s, 6H).

The text of Chapters II, in full, has been submitted for publication. I was the primary researcher and author and the co-authors, Enas A. Mahmoud, Jagadis Sankaranarayanan, José M. Morachis, Carol D. Katayama, Maripat Corr, Stephen M. Hedrick, and Adah Almutairi, directed and supervised the research which forms the basis for this chapter.

Chapter III

Multivalent Porous Silicon Nanoparticles Enhance the Immune Activation Potency of Agonistic CD40 Antibody

Abstract

One of the fundamental paradigms in the use of nanoparticles to treat disease (Peer et al., 2007; Wagner et al., 2006; Gao et al., 2004; Lee et al., 2007) is to evade or suppress the immune system in order to minimize systemic side effects and deliver sufficient nanoparticle quantities to the intended tissues (Peer et al., 2007; Ruoslahti et al., 2010; Moghimi et al., 2001). However, the immune system is the body's most important and effective defense against diseases. It protects the host by identifying and eliminating foreign pathogens as well as self-malignancies. Here we report a nanoparticle engineered to work with the immune system, enhancing the intended activation of antigen presenting cells (APCs). We show that luminescent porous silicon nanoparticles (LPSiNPs), each containing multiple copies of an agonistic antibody (FGK45) to the APC receptor CD40, greatly enhance activation of B cells. The cellular response to the nanoparticle-based stimulators is equivalent to a 30-40 fold larger concentration of free FGK45. The intrinsic near-infrared photoluminescence of LPSiNPs is used to monitor degradation and track the nanoparticles inside APCs.

1. Introduction

Nanomaterials of porous silicon have attracted intense interest for imaging and treatment of diseases including cancer due to their biocompatibility, large specific capacity for drug loading, non-toxic degradation products, and efficient photoluminescence (Park et al., 2009b; Tasciotti et al., 2008; Salonen et al., 2005; Low et al., 2009; Xiao et al., 2011; Wolkin et al., 1999; Canham, 1990; Anderson et al., 2003; Erogbogbo et al., 2008). One of the main barriers to any nanoparticle intended for *in vivo* use is the surveillance by the immune system. For example, the mononuclear phagocyte system (MPS) recognizes and intercepts substantial quantities of systemically administered nanoparticles before they can reach the diseased tissues (Ruoslahti et al., 2010; Moghimi et al., 2001; Park et al., 2009b; Tasciotti et al., 2008; Brigger et al., 2002), and this can lead to significant damage to major organs such as liver, spleen, etc., especially when the nanomaterials carry lethal anticancer drugs. In contrast, approaches to intentionally activate the body's own immune system to fight against diseases can be quite effective (Kantoff et al., 2010; Hodi et al., 2010; Porter et al., 2011; Hunder et al., 2008; Pardoll, 2002; Waldmann, 2003; Rosenberg et al., 2004). The goal of active immunotherapy is to elicit or amplify an immune response to harness the body's inherent defenses against foreign pathogens and self-malignancy. The experimental use of nanomaterials for such active immunotherapies has not been explored to a great extent in part due to the

limited understanding of the interactions between the immune system and nanomaterials (Dobrovolskaia and McNeil, 2007). Nevertheless, recent studies have shown that some nanoparticle-based vaccines can be much more potent than soluble peptide or protein antigens (Shen et al., 2006; Slutter et al., 2010; Uto et al., 2007; Copland et al., 2005; Elamanchili et al., 2004; Cho et al., 2011; Li et al., 2011; Makidon et al., 2008, 2010), and it has been proposed that nanovaccines are more adaptable and perhaps safer than viral vaccines (Peek et al., 2008; Demento et al., 2009; Moon et al., 2011) .

Most studies using nanomaterials in immunotherapies focus on antigen delivery, with little emphasis on the ability of nanomaterials to alter the potency of immunomodulators. In addition, the majority of nanovaccine systems are based on lipids or polymers such as poly(lactic-co-glycolic acid) (PLGA), or polystyrene (Slutter et al., 2010; Uto et al., 2007; Diwan et al., 2003; Petersen et al., 2009; Li et al., 2010; Reddy et al., 2007; Klippstein and Pozo, 2010; Cui et al., 2005), many of which display some intrinsic immune stimulation that may limit their use for immunotherapies (due to unintended stimulation of APCs) or that may interfere with the function of loaded immunomodulators. For many immunotherapeutic or immunomodulation applications, a desirable criterion is that the nanomaterial itself show low intrinsic immune stimulation.

CD40 is a co-stimulatory receptor as well as a member of the family of tumor necrosis factor (TNF) receptors found on APCs such as dendritic cells, B cells, and macrophages (Banchereau et al., 1994; Schoenberger et al.,

1998; Bennett et al., 1998). Agonistic monoclonal antibodies to CD40 (CD40 mAb) can activate APCs and improve immune responses when used in combination with antigens or vaccines (Pardoll, 2002; Dougan and Dranoff, 2009; Palucka et al., 2010). In addition, CD40 mAb can produce substantial antitumor efficacy and can also potentially be used to treat chronic autoimmune inflammation (Beatty et al., 2011; Vonderheide et al., 2007; Jackaman et al., 2011; Mauri et al., 2000). However, the therapeutically effective dose of CD40 mAb is high and the high dose can result in severe side effects (Jackaman et al., 2011; Barr et al., 2003). We have recently developed nanoparticles based on luminescent porous silicon that display low systemic toxicity and degrade *in vivo* into renally cleared components (Park et al., 2009b; Heinrich et al., 1992; Gu et al., 2010). The porous nanostructure and intrinsic near-infrared photoluminescence of porous silicon nanoparticles (LPSiNPs) enable the incorporation of drug payloads and the monitoring of distribution and degradation *in vivo* (Park et al., 2009b). In this study, we show that when multiple copies of the CD40 mAb FGK45 are incorporated onto a LPSiNP, the activation potency on B cells is significantly amplified, equivalent to using ~ 30-40 fold larger concentration of free FGK45. LPSiNPs without FGK45 appear inert to B cells.

2. Results

LPSiNPs were prepared by electrochemical etch of highly doped p-type single-crystal Si wafers in an electrolyte consisting of aqueous hydrofluoric acid and ethanol, lift-off of the porous layer, ultrasonic fracture, filtration of the resulting nanoparticles through a 0.22 μm filter membrane, and finally activation of luminescence by treatment in an aqueous solution following the published procedure (Park et al., 2009b; Heinrich et al., 1992; Gu et al., 2010). To incorporate FGK45 onto the nanoparticles, we first coated the LPSiNPs with avidin by physisorption (av-LPSiNPs). Biotinylated FGK45 was then conjugated to the nanoparticles through the strong biotin-avidin binding interaction (FGK-LPSiNPs), Fig. 1a. Approximately 0.058mg of FGK45 was loaded per milligram of LPSiNPs, as measured by bicinchoninic acid (BCA) protein assay. The structure of FGK45 loaded on nanoparticle-FGK45 construct was also confirmed by gel electrophoresis and immunoblotting (Fig 5). The FGK-LPSiNPs appeared similar to LPSiNPs in the transmission electron microscope (TEM) images (Fig. 1b), but the mean hydrodynamic size measured by dynamic light scattering (DLS) increased from ~ 130 ± 10 nm to ~ 188 ± 15 nm after protein attachment (Fig 6).

The intrinsic photoluminescence from the silicon nanostructures in FGK-LPSiNPs under ultraviolet excitation appeared in the near-infrared region of the spectrum (λ_{max} = 790 nm), similar to the non-loaded LPSiNPs. However, the intensity of photoluminescence was somewhat lower from the

protein-coated formulation (Fig 1c) (Park et al., 2009b). In a physiologically relevant aqueous solution of phosphate buffered saline (PBS) at pH 7.4 and 37 °C, the FGK-LPSiNP construct was observed to degrade within 24 h (Fig. 1d). The degradation was tracked by monitoring disappearance of the photoluminescence signal, which decreased gradually upon dissolution of the quantum confined silicon nanostructure (Canham, 1990; Lehmann and Gosele, 1991), and by appearance of free silicic acid in solution (by inductively coupled plasma-optical emission spectroscopy, ICP-OES), Fig. 1d.

The FGK-LPSiNPs were more readily taken up by APCs compared to bare LPSiNPs. When cultured with mouse bone marrow-derived dendritic cells (BMDC), LPSiNPs showed limited (but still detectable) presence in the cells (Fig. 2a); in contrast, BMDC incubated with FGK-LPSiNPs under the same conditions showed much higher uptake of nanoparticles (Fig. 2b). This uptake was substantially blocked by pre-treatment of the BMDC with free FGK45 (Fig 2c), indicating that FGK45 binding to the BMDC was responsible for the increased internalization of FGK-LPSiNP. It has been shown that CD40 ligand and agonistic antibodies can induce CD40 endocytosis upon binding (Chen et al., 2007, 2006) , which may be responsible for uptake of FGK-LPSiNP in the present case. Interaction of Fc receptors of BMDC with the Fc region of FGK45 antibody could also have contributed to the uptake. As reported by Li and Ravetch, agonistic CD40 antibodies also engage FcγRIIB on APCs (Li and Ravetch, 2011). Pre-incubation of BMDC with anti-

mouse FcγRII-III prior to FGK-LPSiNP somewhat reduced, but did not eliminate, uptake of the nanoparticles (Fig 7).

Subcellular localization of FGK-LPSiNPs was further examined by confocal fluorescence microscopy. By following the near-infrared photoluminescence spectrum of the nanoparticles, we visualized FGK-LPSiNPs outside of the lysosomes of the dendritic cells (Fig. 2d). This finding is consistent with previous reports that various types of silicon or silica based nanomaterials can escape from lysosomes and distribute inside the cytosol (Park et al., 2009b; Slowing et al., 2006; Serda et al., 2009; Ashley et al., 2011). Although LPSiNPs are expected to degrade within a few hours at pH 7.4 due to dissolution of the protective oxide coating (Park et al., 2009b; Wu et al., 2008), they are much more stable in acidic environments similar to the interior of lysosomes. In the present case, less than 5% of the nanoparticles dissolved over 24 h in pH 4 buffer solution (Fig. 2e and Fig 8).

We next investigated the activity of FGK-LPSiNPs added to B cells, by measuring the expression of cell surface molecules indicative of B cell activation. The nanoparticles in this experiment contained avidin labeled with fluorescein isothiocyanate (avidin-FITC). The resulting construct emits both in the green (from the FITC label) and in the near-infrared (from the silicon nanostructure) when excited with ultraviolet light (Fig. 3a). B cells enriched from mouse splenocytes were incubated with FGK-LPSiNPs or av-LPSiNPs and then analyzed by flow cytometry. After 42 h of culture, the FITC signal

was only detected from B cells that had been exposed to FGK-LPSiNPs (Fig. 3b-e). B cells incubated with FGK-LPSiNPs also displayed increased expression of the cell surface receptors, CD86 and MHC II, the response typical of B cells that have received a signal through CD40 (Fig. 3b-e) (Beatty et al., 2011).

Furthermore, the extent of activation induced by FGK-LPSiNPs was concentration dependent (Fig 9). When exposed to a low concentration of FGK-LPSiNPs, not all of the B cells were activated, as indicated by the wide distribution of the fluorescence intensity from the cells in flow cytometry dot plots (Fig 3b, 3d). However, the population of B cells that displayed high FITC signals also expressed high levels of CD86 and MHC II, indicating that the cells bound with nanoparticles were the ones that upregulated their activation markers (Fig 3b, 3d). In contrast, B cells cultured with various concentrations of av-LPSiNP all showed low FITC signals and low activation marker levels (Fig 10).

Multivalency is one of the notable advantages of using nanomaterials for biomedical applications. For example, studies using nanoparticles as cancer diagnostic and therapeutic agents have shown that when multiple copies of tumor targeting ligand are displayed on an individual nanoparticle, its tumor targeting efficiency can be significantly enhanced (Hong et al., 2007; Park et al., 2009a; Liu et al., 2007; Montet et al., 2006). This enhancement is generally ascribed to the multivalent effect which is also observed in many

natural processes such as antibody interactions and clotting interactions (Ruoslahti et al., 2010). To determine if multivalency plays a strong role in the activation potency of the agonistic antibody to APCs, we cultured B cells with either FGK-LPSiNPs or an equivalent concentration of free FGK45 and analyzed the cells by flow cytometry. Both FGK-LPSiNPs and free FGK45 activated B cells, and the activation level of the cells correlated with the concentration of FGK45 (Fig. 4a). However, at a given total concentration of FGK45 antibody, FGK-LPSiNPs showed substantially higher activation potency than free FGK45. Activated B cells upregulated CD86 and MHC II to a detectable level when cultured with FGK-LPSiNPs containing as little as ~3.6-7.2ng/mL of FGK45; whereas a similar level of B cell activation was only observed when the concentration of free FGK45 was ≥140 -200 ng/mL (Fig. 4a). Comparison of the titration curves of FGK-LPSiNPs and free FGK45 revealed that the B cell activation potency of FGK45 in the FGK-LPSiNP constructs is equivalent to using ~30-40 fold larger concentration of free FGK45 (Fig. 4a).

To test if the enhancement of APC activation is caused by the uncoated porous silicon nanomaterial itself, we cultured B cells with various concentrations of LPSiNPs as control experiments. No induction of CD86 or MHC II was observed at all tested LPSiNP concentrations (up to 5000 ng/mL, equivalent to the highest concentration of FGK-LPSiNPs used in the stimulation study). This suggests that the amplification induced by the FGK-

LPSiNP construct results from enhancement of the agonistic antibody's intrinsic function rather than an immune response from the nanomaterial itself (Fig. 4b and Fig 11). The very low stimulation of APC by LPSiNPs is attributed to their primarily inorganic chemical composition; their chemical structure and biodegradation products possess little similarity to natural pathogens or other "danger signals" normally presented to the immune system (Anderson et al., 2003; Dobrovolskaia and McNeil, 2007; Van Dyck et al., 2000).

3. Conclusion

This study represents the first example of a nanoparticle that amplifies APC activation potency of an agonistic CD40 antibody. In addition to the enhancement effect, the inert inorganic composition and biodegradable property of LPSiNPs could overcome some of the disadvantages of lipid or polymer-based materials for immunotherapy applications. Their intrinsic photoluminescence also provides a means to monitor the degradation of LPSiNPs and track their interaction with the immune system. The amplifying effect and the synthetic versatility of the silicon nanomaterial provide a promising means to develop immunomodulators or nanovaccines.

4. Methods

4.1. Preparation of FGK45 loaded luminescent porous silicon nanoparticles (FGK-LPSiNPs)

LPSiNPs were first prepared using a previously described method (Park et al., 2009b; Sailor, 2012). In brief, (100)-oriented p-type single-crystal Si wafers (0.8-1.2 mΩ cm, Siltronix) were electrochemically etched in an electrolyte containing aqueous 48% hydrofluoric acid and ethanol in a 3:1 ratio. The resulting porous Si films were lifted from the Si substrate, fractured by ultrasound and filtered through a 0.22 um membrane. Finally, the photoluminescence of the nanoparticles were activated by soaking in deionized water for 14 d. To prepare FGK-LPSiNP, an avidin coating was first applied. A 1 mL aliquot of an aqueous dispersion of 0.2 mg of LPSiNP was mixed with a 0.08 mL aliquot of water containing 0.04 mg of avidin (Thermo Fisher Scientific, Inc.). The mixture was stirred for 1 h at room temperature, rinsed with water three times by centrifugation. The particles were resuspended in water to 0.2 mg/mL and were then mixed with a 0.045 mL aliquot of water containing 0.022 mg of biotin conjugated FGK45 (Enzo Life Sciences, Inc.). The mixture was stirred for 1 h at room temperature, rinsed with water three times by centrifugation to remove any excess FGK45. The supernatant of each wash was combined and the quantity of excess FGK45 in the supernatant was measured by micro BCA (bicinchoninic acid) protein

assay (Thermo Fisher Scientific, Inc.) to calculate the quantity of FGK45 loaded on LPSiNP.

4.2. Nanoparticle characterization

Transmission electron micrographs (TEM) were obtained with a FEI Tecnai G^2 Sphera. Dynamic light scattering (Zetasizer Nano ZS90, Malvern Instruments) was used to determine the hydrodynamic size of the nanoparticles. The photoluminescence (PL, λ_{ex} = 370 nm and 460 nm long pass emission filter) spectra of LPSiNP or FGK-LPSiNP were obtained using a Princeton Instruments/Acton spectrometer fitted with a liquid nitrogen-cooled silicon charge-coupled device (CCD) detector.

4.3. In vitro degradation of FGK-LPSiNP

A series of samples containing 0.05 mg/mL of FGK-LPSiNP in 1 mL of PBS solution or pH 4.0 buffer solution were incubated at 37 ºC. An aliquot of 0.5 mL of solution was removed at different time points and filtered with a centrifugal filter (30,000 Da molecular weight cut-off, Millipore, inc.) to remove undissolved LPSiNP. 0.4 mL of the filtered solution was diluted with 5 mL HNO_3 (2%(v/v)) and subjected to analysis by inductively coupled plasma optical emission spectroscopy (ICP-OES, Perkin Elmer Optima 3000DV). The decrease in PL of the above samples over time was also monitored.

4.4. Mice

C57BL/6 mice were maintained in specific pathogen-free facilities at the University of California, San Diego. Animal protocols were approved by the Institutional Animal Care and Use Committee.

4.5. Cell uptake of FGK-LPSiNP

Mouse bone marrow-derived dendritic cells (BMDC) were prepared as described (Dejean et al., 2009) and harvested on day 8 for use in microscopy experiments. BMDC (40,000-60,000 cells per well) were seeded into 8-well chamber glass slides (Millipore, inc.) and cultured overnight. The cells were washed with RPMI (Roswell Park Memorial Institute) medium once and incubated with 0.05 mg/mL LPSiNP or FGK-LPSiNP in RPMI medium for 1.5 hours at 37^{o}C. For the competitive binding experiment, BMDC were first incubated with 0.03 mg/ml free FGK45 for 30 min in RPMI medium, then incubated with 0.05 mg/mL FGK-LPSiNP as above. The cells were washed 3 times with RPMI medium and incubated with Alexa Fluor 488 conjugated CD11c antibody (clone N418, eBioscience—all antibodies are from eBioscience unless otherwise indicated; 1µg/ml) in RPMI medium for 10 min to visualize the BMDC. The cells were then rinsed three times with PBS, fixed with 4% paraformaldehyde for 20 min and then observed with a Zeiss LSM 510 confocal fluorescence microscope. An excitation wavelength of 405 nm

and an emission filter with a bandpass at 700 ± 50 nm were used to image the near-IR photoluminescence of the nanoparticles.

4.6. In vitro stimulation of B cells

Single-cell suspensions of C57BL/6 splenocytes were prepared and subjected to red blood cell lysis using ACK lysis buffer (0.15 *M* NH_4Cl, 1 m*M* $KHCO_3$, 0.1 m*M* EDTA, pH 7.3). B cells were sorted out via CD43 (Miltenyi Biotec) magnetic bead depletion. Sorted cells were plated at $2x10^5$ cells/well and incubated with LPSiNP, av-LPSiNP, FGK-LPSiNP, free agonistic anti-CD40 (clone FGK45), PBS, or CpG (Pfizer) for 42 h at 37 °C.

4.7. Flow cytometry

Approximately 1-2 million cells were resuspended in Hank's Balanced Salt Solution (Invitrogen) with 1% fetal calf serum (Omega Scientific) added (HBSS 1% FCS), incubated for 15 min at 4 °C with anti-mouse FcγRII-III (supernatant from hybridoma 2.4G2 cultures), and stained with fluorescently conjugated antibodies for 20 min at 4ºC. For particles using avidin-FITC, cells were stained with MHC II biotin (M5/114.15.2), washed with HBSS 1% FCS, stained with streptavidin PerCP, CD86 Phycoerythrin (GL1; PE) and B220 Allophycocyanin (RA3-6B2) and analyzed by flow cytometry. For particles using non-labeled avidin, cells were stained with B220 FITC, CD86 PE and MHC II Allophycocyanin and analyzed by flow cytometry.

Acknowledgements

This work was supported by the National Cancer Institute of the National Institutes of Health through grant numbers U54 CA 119335 (UCSD CCNE) and 5-R01-CA124427 (BRP), and by the National Science Foundation under Grant No. DMR-0806859. L.G. was partially supported by the UCSD HHMI/NIBIB Interfaces Graduate Training Program (HHMI grant HHMI56005681). L.E.R. was supported by University of California, San Diego Immunology training grant NIH T32AI060536-02. The authors thank the National Center for Microscopy and Imaging Research (NCRR Grant 5P41RR004050) for use of their facilities.

Author Contributions

L.G., L.E.R., S.M.H., and M.J.S. conceived and designed the research. L.G., L.E.R., and Z.Q. performed the experiments. L.G., L.E.R., Z.Q., M.P.C., S.M.H., and M.J.S. analyzed the data. L.G., L.E.R., M.P., S.M.H., and M.J.S. wrote the manuscript.

Competing Interests Statement

The authors declare no competing financial interests.

Figures

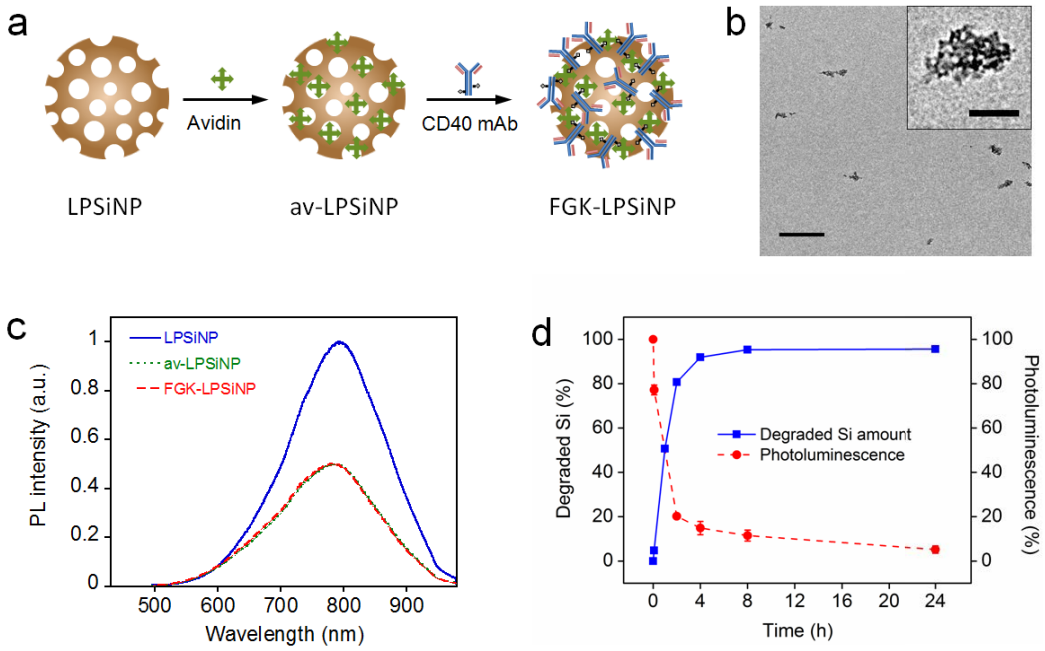

Figure 1. Preparation and characterization of FGK45 loaded luminescent porous silicon nanoparticles (FGK-LPSiNP). a, Schematic representation of the preparation of FGK-LPSiNP. LPSiNP was first coated with avidin by physisorption (av-LPSiNP). Biotinylated FGK45 was then conjugated to the nanoparticles through biotin-avidin binding to form FGK-LPSiNP. **b,** Transmission electron microscope image of FGK-LPSiNP (inset shows the porous nanostructure of one of the nanoparticles). Scale bar is 1 μm (100 nm for the inset). **c,** Photoluminescence (PL) spectra of LPSiNP, av-LPSiNP and FGK-LPSiNP. PL was measured using UV excitation (λ_{ex}= 370 nm). **d,** Appearance of dissolved silicon in solution (by ICP-OES) and decrease in photoluminescence intensity from a sample of FGK-LPSiNP (50 μg/mL) incubated in PBS solution at 37^{o}C as a function of time.

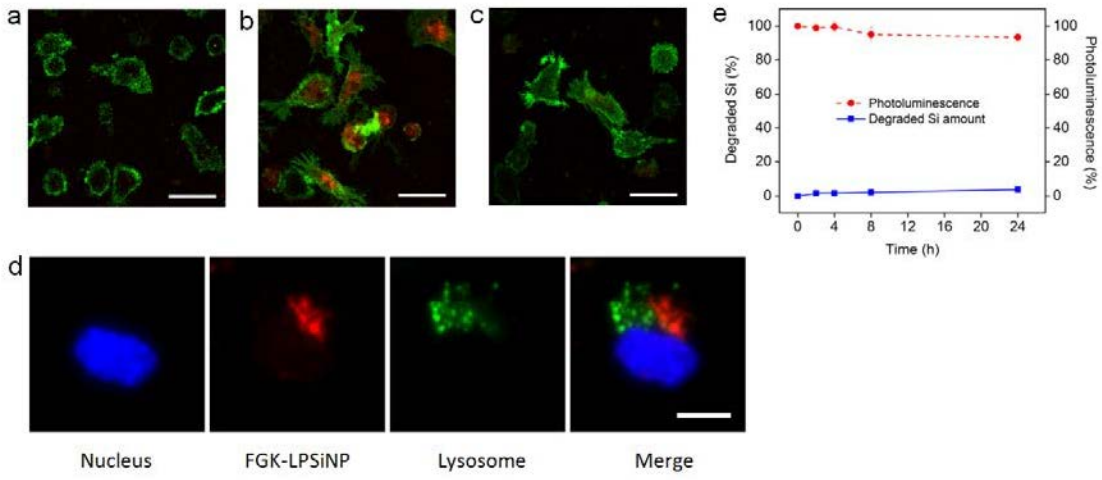

Figure 2. Dendritic cell uptake of FGK-LPSiNPs. Fluorescence microscope images of mouse bone marrow-derived dendritic cells (BMDC) incubated with (**a**) LPSiNPs or (**b**) FGK-LPSiNPs for 1.5 h at 37 °C. **c**, Free FGK45 inhibits uptake of FGK-LPSiNPs. BMDC were blocked with free FGK45 for 30 min and then incubated with FGK-LPSiNPs for 1.5 h at 37 °C. BMDC were detected by staining with Alexa Fluor 488 conjugated CD11c antibody (green). FGK-LPSiNPs were detected by their intrinsic visible/near-infrared photoluminescence (red, λ_{ex}= 405 nm and λ_{em}= 700 ± 50 nm). The scale bars are 40 μm. **d**, FGK-LPSiNPs distribution in BMDC. BMDC were incubated with FGK-LPSiNP for 1.5 h at 37 °C. The lysosomes (green) of the cells were stained with LysoTracker (Invitrogen). Blue and red indicate the cell nucleus and FGK-LPSiNPs, respectively. The scale bar is 10 μm. **e,** Degradation of LPSiNPs (50 μg/mL) in pH 4 buffer solution at 37 °C as a function of time.

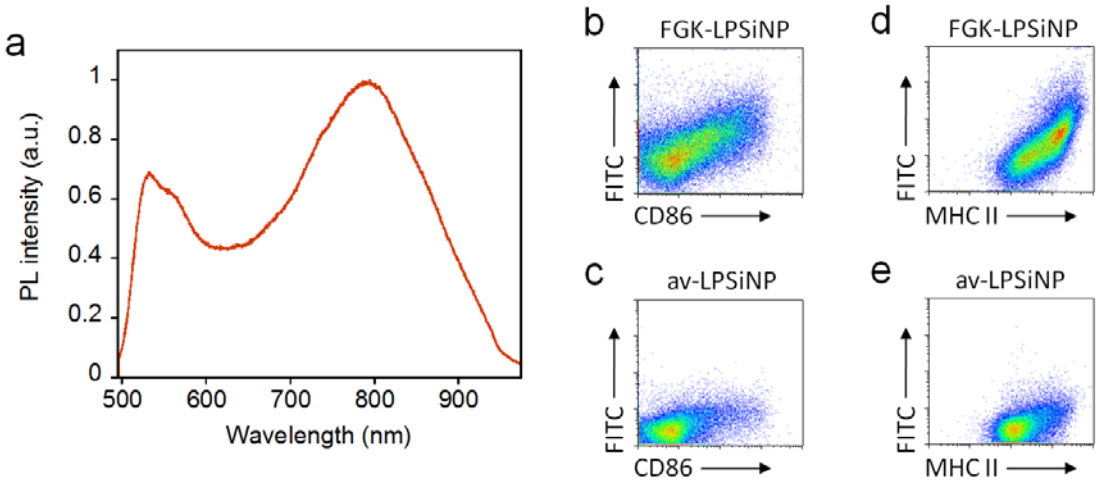

Figure 3. Interaction of FGK-LPSiNPs with B cells. a, Photoluminescence spectrum of LPSiNPs coated with FITC-labeled avidin, showing the emission bands from both the FITC label (λ_{max} ~ 520 nm) and porous silicon (λ_{max} ~790 nm). **b-e,** Flow cytometry data quantifying the level of expression of the B cell activation markers CD86 (**b, c**) and MHC II (**d, e**) after incubation with 5 μg/mL of FGK-LPSiNPs (**b, d**) or av-LPSiNPs (**c, e**) for 42 h. The nanoparticles used in this experiment were coated with FITC-labeled avidin. The FITC signal from the cells is plotted against the expression level of CD86 (**b, c**) or MHC II (**d, e**) after stimulation. FGK-LPSiNPs used here contain 36 μg of FGK45 per milligram of nanoparticles. Note the quantity of FGK45 loaded is smaller when LPSiNPs are coated with FITC conjugated avidin compared with non-labeled native avidin.

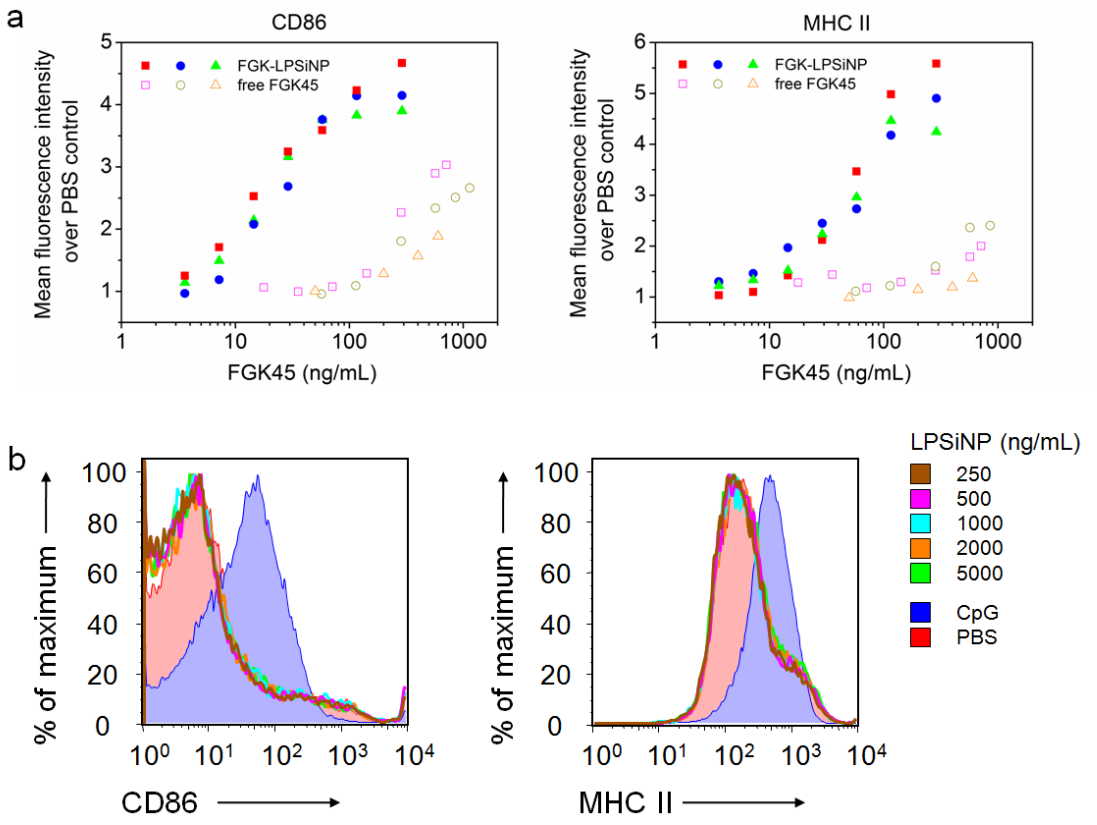

Figure 4. Amplified activation potency of FGK-LPSiNPs compared to free FGK45. **a**, Flow cytometry analysis of the expression of B cell activation markers CD86 and MHC II, represented as the relative mean fluorescence intensity of the marker staining, after incubation with either FGK-LPSiNPs or free FGK45 for 42 h at 37 °C. The concentration of FGK45 on the FGK-LPSiNP constructs is reported based on the total loading of FGK45 on the nanoparticles (58 μg of FGK45 per mg of nanoparticles). Data are from independent experiments. **b,** Flow cytometry histograms of B cell activation markers CD86 and MHC II after incubation with various concentrations of LPSiNPs for 42 h at 37 °C. PBS (red shaded) and CpG (blue shaded) were used as negative and positive controls, respectively.

Supplementary information:

5. Supplemental Methods

5.1. Immunoblot analysis

FGK-LPSiNPs and FGK45 were diluted in lithium dodecyl sulfate (LDS) sample buffer and reducing agent (Invitrogen), incubated at 80 °C for 10 min, loaded on a 4-12% Bis-Tris gel (Invitrogen) and run under reducing conditions. The gel was then transferred to PVDF membrane and a western blot was performed to detect rat IgG. Briefly, the membrane was blocked in 5% milk in tris-buffered saline Tween 20 (TBST) for 30 min, probed with goat anti-rat IgG (H+L) HRP (Southern Biotech, diluted 1:10,000 in 5% milk in TBST) for 60 min, washed three times with TBST, prepared with ECL Plus substrate (Amersham Biosciences) and signal was detected on a Typhoon 9400 variable mode imager (Amersham Biosciences).

5.2. Photoluminescence measurement of LPSiNPs in acidic buffer solutions

LPSiNPs were suspended in pH 3, 4 or 5 buffer solutions (VWR International, LLC) at a concentration of 0.05 mg/mL. The photoluminescence (PL, λ_{ex} = 370 nm and 460 nm long pass emission filter) spectra of LPSiNPs in various pH buffer solutions were obtained using a Princeton Instruments/Acton

spectrometer fitted with a liquid nitrogen-cooled silicon charge-coupled device detector.

5.3. In vitro stimulation of B cells

Single-cell suspensions of C57BL/6 splenocytes were prepared and subjected to red blood cell lysis using ACK lysis buffer (0.15 *M* NH_4Cl, 1 m*M* $KHCO_3$, 0.1 m*M* EDTA, pH 7.3). B cells were sorted out via CD43 (Miltenyi) magnetic bead depletion. Sorted cells were plated at $2x10^5$ cells/well and incubated with LPSiNP, av-LPSiNP, FGK-LPSiNP, free agonistic anti-CD40 (clone FGK45), PBS, or CpG (Pfizer) for 42 h at 37 °C.

5.4. Flow cytometry

Approximately 1-2 million cells were resuspended in Hank's Balanced Salt Solution (Invitrogen) with 1% fetal calf serum (Omega Scientific) added (HBSS 1% FCS), incubated for 15 min at 4 °C with anti-mouse FcγRII-III (supernatant from hybridoma 2.4G2 cultures), and stained with fluorescently conjugated antibodies for 20 min at 4ºC. For particles using avidin-FITC, cells were stained with MHC II biotin (M5/114.15.2), washed with HBSS 1% FCS, stained with streptavidin PerCP, CD86 Phycoerythrin (GL1; PE) and B220 Allophycocyanin (RA3-6B2) and analyzed by flow cytometry. For particles using non-labeled avidin, cells were stained with B220 FITC, CD86 PE and MHC II Allophycocyanin and analyzed by flow cytometry.

Supplemental Figures

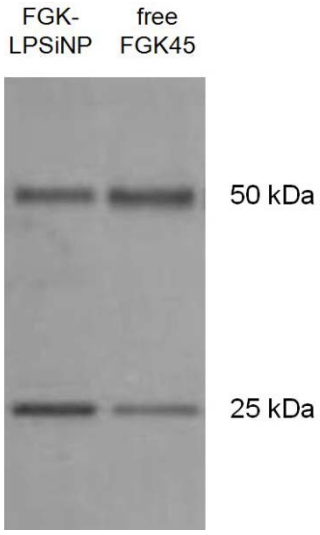

Figure 5. Immunoblot analysis of FGK45 loaded on luminescent porous silicon nanoparticles (LPSiNPs). A western blot used to detect rat IgG (H+L) in FGK-LPSiNPs and free FGK45 is shown. The gel was run under reducing conditions, yielding both heavy (50kDa) and light (25kDa) chain antibody bands of FGK45. Antibody that had been loaded on LPSiNPs appears similar to free FGK45.

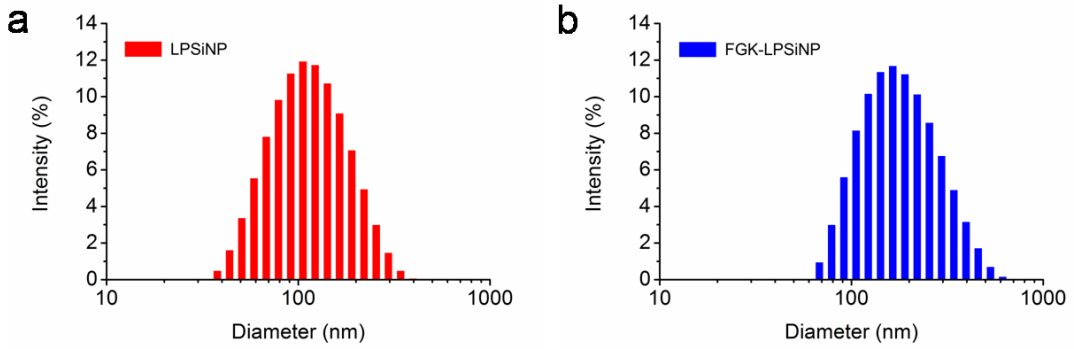

Figure 6. Representative hydrodynamic size data. Hydrodynamic size distribution of (**a**) LPSiNPs and (**b**) FGK-LPSiNPs obtained by dynamic light scattering. Note that the mean size increases from ~130 nm to ~188 nm due to the attached protein molecules.

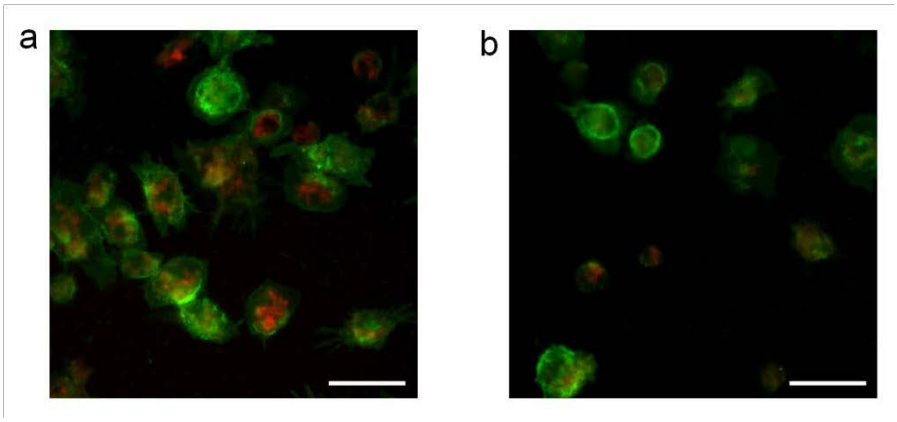

Figure 7. Dendritic cell uptake of FGK-LPSiNPs. Fluorescence microscope images of mouse bone marrow-derived dendritic cells (BMDC) incubated with FGK-LPSiNPs for 1.5 h at 37 °C. **a**, BMDC were incubated with FGK-LPSiNPs directly. **b**, BMDC were blocked with anti-mouse FcγRII-III for 30 min prior to incubation with FGK-LPSiNPs. BMDC were detected by staining with Alexa Fluor 488 conjugated CD11c antibody (green). FGK-LPSiNPs were detected by their intrinsic visible/near-infrared photoluminescence (red, λ_{ex}= 370 nm and λ_{em}= 720 ± 80 nm). The scale bars are 40 μm.

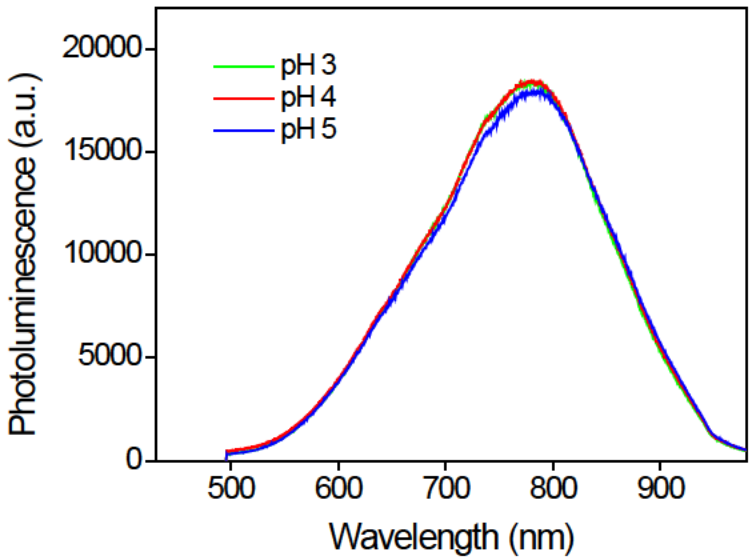

Figure 8. Photoluminescence spectra of LPSiNPs in acidic buffer solutions at room temperature. The nanoparticles are stable in all three acidic pH values indicated (excitation wavelength 370 nm, emission filter 460 nm longpass).

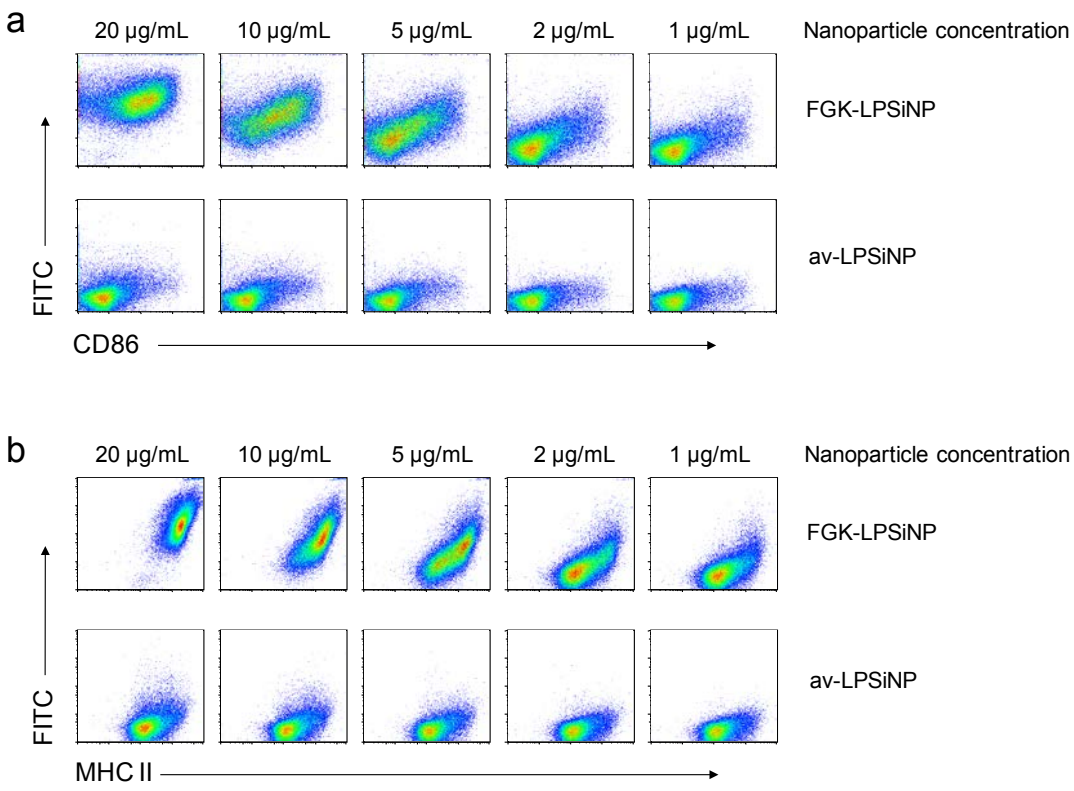

Figure 9. Stimulation of B cells using various concentrations of FGK45 loaded LPSiNPs (FGK-LPSiNPs, top row in (a) and (b)) or avidin coated LPSiNPs (av-LPSiNPs, bottom row in (a) and (b)). FGK-LPSiNPs used in this study contain 0.036 mg of FGK45 in 1 mg of nanoparticles. Avidin was conjugated with FITC before coating on the nanoparticles. After 42 h of culture, the FITC signal is only detected from B cells that had been stimulated with FGK-LPSiNPs. The B cells stimulated with FGK-LPSiNPs upregulated the activation markers CD86 (**a**) and MHC II (**b**), and the cells with high FITC signal also expressed high levels of CD86 (**a**) and MHC II (**b**), which indicates the cells that bound FGK-LPSiNPs were also the ones that upregulated the activation markers.

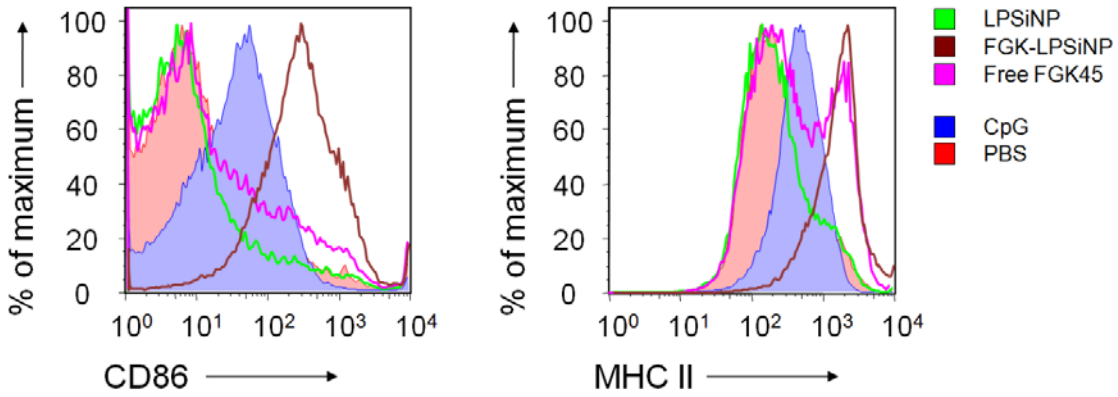

Figure 10. No CD86 or MHC II upregulation of B cells incubated with LPSiNP. Flow cytometry histograms of B cell activation markers CD86 and MHC II after incubation with 5 μg/mL of LPSiNPs (green curve), 5 μg/mL of FGK-LPSiNPs containing 0.29 μg of FGK45 (maroon curve), or 0.29 μg of free FGK45 (magenta curve) for 42 h at 37 °C. PBS (red shaded) and CpG (blue shaded) were used as negative and positive controls, respectively.

Antibody-OVA LPSiNPs Target and Activate APCs *in vitro*, but Fail to be Effective Long-Term *In vivo*

6. Introduction

In addition to silicon nanoparticles displaying FGK, we also produced and tested nanoparticles displaying both antigen and targeting antibodies. For targeting, we used full-length DEC205 antibody, with whole ovalbumin incorporated at the 3' end of the Fc region as the antigen (DEC-OVA). This antibody-OVA hybrid was first described a decade ago (Hawiger et al., 2001), and may now be produced by transfection of heavy and light chain antibody plasmids into 293T cells. As a control, anti-hemagluttinin (HA) antibody was expressed with OVA in a similar manner (HA-OVA). LPSiNPs were made with antibody-OVA only or antibody-OVA and agonistic CD40 antibody (FGK; Enzo Life Sciences) on the same particle. *In vitro* results indicated the nanoparticles containing DEC-OVA did target antigen to APCs better than HA-OVA, and nanoparticles containing FGK could all induce upregulation of CD86 and MHC II on B cells. Short-term T cell proliferation was observed *in vivo* with nanoparticles containing DEC-OVA, however, by two weeks post-vaccination, these cells seemed to be undergoing deletion, even when the particle also displayed FGK.

7. Methods and Results

7.1. Molecular cloning

cDNA was purified from hybridomas expressing the HA and CD40 antibodies (clones: 12CA5 and FGK). Variable region heavy chain (VH) or variable region kappa light chain (VL)-specific PCRs were performed for HA. Constant region light chain (CL, kappa light chain)-specific PCR for CD40 antibody was done. Anti-HA VH was cloned in frame into the pFuse-CHIg-mIgG2a vector (Invivogen), directly in front of the CH. The pFuse-CHIg-mIgG2a vector expresses the full-length constant region of mIgG2a heavy chain antibody (CH), preceded by a multicloning site for insertion of VHs. The light chain was also expressed in the pFuse vector, with all CH inserts removed. The CL from anti-CD40 was cloned into the multi-cloning site, directly preceded, in frame, with anti-HA VL. The VH and VL constructs were both inserted with their leader sequences intact, meaning upon transfection, the antibody constructs were secreted. Finally, whole OVA was cloned by PCR from OVA cDNA (Dr. Marc Jenkins, University of Minnesota, Twin Cities), given a 5' linker sequence, and inserted in frame, following the CH region of the heavy chain construct. A biotinylation site (BirA) was also added at the 3' end of this construct. This allows biotinylation of the vaccine construct and subsequent multimerization. A schematic of the proposed plasmids is presented in Figure 11A.

DEC-OVA heavy and light chain plasmids in the pRKW2 vector were obtained from Dr. Michel Nussenzweig (Rockefeller University, New York). Light chain plasmid was not altered. Heavy chain plasmid alteration removed the stop codon directly after the OVA, inserted a BirA site 3' of OVA, and inserted a stop codon 3' of the BirA site. To accomplish this, a 250bp fragment was cloned by PCR from the HA-OVA heavy chain plasmid and inserted into the DEC-OVA heavy chain plasmid. The 5' end of the fragment begins at a unique EcoRV site in OVA. The 3' end contains the BirA site, followed by a stop codon and a Not I site, which is unique in the pRKW2-DEC205 heavy chain plasmid and occurs 3' of OVA and the original stop codon.

7.2. Protein expression and purification

Protein was expressed in the mammalian 293T cell line by transient co-transfection of VH (expressing full-length OVA) and VL constructs with polyethylenimine (Sigma). Supernatant was collected and the expressed protein was purified via protein G columns (GE Healthsciences). Purified constructs were biotinylated at the BirA site in their heavy chains with BirA enzyme (Avidity). Constructs were then quantitated by BCA assay and conjugated to avidin-coated LPSiNPs with or without biotinylated FGK (Fig 11B) in the same manner as described previously in this chapter (Fig 1A).

Verification of constructs' production was done by western blot, protein gel, and cell staining. Western blot for heavy chain, light chain, and OVA was

done on supernatants from transfected 293T cells, under both reducing (Fig 11C) and non-reducing (not shown) conditions to verify full length expression and heavy and light chain assembly. A 4-12% Bis-Tris gel (Invitrogen) was run under reducing conditions to verify purity of the protein preparations (Fig 11D). To verify functional binding specificity, splenocytes were stained with one of the antibody-OVA constructs, followed by rabbit anti-OVA secondary antibody (Chemicon) and anti-rabbit FITC (BD Pharmingen) tertiary antibody (Fig 11E). B220 PE and CD11c Allophycocyanin staining was also done. As expected, HA-OVA did not stain B cells or DCs, and DEC-OVA stained both.

7.3. In vitro testing

Next, antibody-OVA LPSiNPs (with or without FGK conjugated) were tested *in vitro* for their ability to stimulate and deliver antigen to APCs. Splenic B cells were sorted via CD43 magnetic bead depletion (Miltenyi Biotec) and incubated with 5-fold dilutions of the purified protein constructs (highest dose: 20μg/ml particle) for two days at 37ºC (Fig 12A). Free FGK was also done for comparison. Stimulation of B cells was detected by upregulation of CD86 (CD86 PE) and MHC II (MHC II Allophycocyanin). All LPSiNPs displaying FGK induced upregulation of the markers to a similar extent. The dose of FGK required for activation was ~5-fold less on the particles than free FGK. HA-OVA LPSiNPs and DEC-OVA LPSiNPs did not induce upregulation.

Antibody-OVA LPSiNPs were next tested for their ability to deliver antigen to APCs. Bone marrow cells were cultured for 9 days in GM-CSF as

described (Dejean et al., 2009) to generate bone marrow derived DCs (BMDCs). 10,000 BMDCs were plated/well in a 96-well round bottom plate in complete media and incubated for 1 day with nanoparticles. Nanoparticles were: 1 or 10μg/ml of LPSiNP, av-LPSiNP (LPSiNP coated with avidin only), FGK LPSiNP, HA-OVA LPSiNP, HA-OVA FGK LPSiNP, DEC-OVA LPSiNP, DEC-OVA FGK LPSiNP, and FGK LPSiNP. Non-nanoparticle vaccines were also used in doses similar to the amount on the nanoparticles: 50 or 500ng/ml HA-OVA or DEC-OVA (± 35 or 350ng/ml FGK). Finally, controls of PBS, LPS+OVA, FGK (35 or 350ng/ml) + OVA (16.8 or 168ng/ml), and FGK (35 or 350ng/ml) were included.

After 1 day, cells were washed twice and incubated with 250,000 carboxyfluorescein succinimidyl ester (CFSE)-labeled CD4+ OT-II T cells or CD8+ OT-I T cells. The T cells and BMDCs were incubated at 37ºC for 2 days, then washed and stained with CD69 PE (1.2H3) and CD4 or CD8 Allophycocyanin and analyzed by flow cytometry (Fig 12B). All DEC-OVA treatments (antibody or LPSiNP, ±FGK) induced upregulation of CD69 and CFSE dilution (proliferation) for CD4 T cells. A similar result was observed for CD8 T cells, except that DEC-OVA LPSiNP without FGK did not induce either CD69 upregulation or CFSE dilution.

7.4. In vivo testing

LPSiNPs were tested *in vivo* for ability to induce T cell proliferation. CD45.1 mice were injected with $1x10^6$ CFSE-labeled OT-I CD8+ T cells

(CD45.2 background) i.v. One day later, mice were immunized (3 mice/group) with 1μg or 5μg of HA-OVA LPSiNP, HA-OVA FGK LPSiNP, DEC-OVA LPSiNP, or DEC-OVA FGK LPSiNP in the footpad s.c. Also, one mouse was given PBS and one mouse was given 10μg LPS + 50μg OVA. Three days post-immunization, mice were sacrificed and spleen, inguinal lymph nodes, and popliteal lymph nodes were taken, counted, stained, and analyzed by flow cytometry. Stains were CD8 PerCP and CD45.2 PE (104). Both LPSiNPs containing DEC-OVA showed increased CD8 T cell proliferation in all organs (Fig 13A), more notably in the inguinal LN and spleen. The popliteal lymph node is the draining lymph node, and therefore, all OVA-containing vaccinations did induce some proliferation in this organ. Total numbers of CD45.2+CD8 T cells were also increased in the 5μg DEC-OVA LPSiNP and 5μg DEC-OVA FGK LPSiNP vaccinations, most notably in inguinal LN (1-2 x 10^4 cells vs 1-1.3 x 10^3 cells for HA-OVA LPSiNP or HA-OVA FGK LPSiNP; Fig 13A).

To examine the immune response at a later timepoint, CD45.1 mice were again given 1x10^6 CD45.2 OT-I CD8 T cells i.v. and immunized with LPSiNPs s.c. 1 day later. Nanoparticles given were: HA-OVA LPSiNP, HA-OVA FGK LPSiNP, DEC-OVA LPSiNP, or DEC-OVA FGK LPSiNP, all at 24μg dosage. Individual antibodies and controls were also given as follows: 4μg HA-OVA ± 100μg FGK, 4μg DEC-OVA ± 100μg FGK, PBS and 10μg LPS + 100μg OVA. Mice were sacrificed at day 13 post-vaccination and inguinal,

axillary, and brachial lymph nodes and spleen were taken. Cells were stained with B220 FITC, CD11b FITC, Ter119 FITC, CD4 FITC, CD45.2 Pacific Blue, CD44 APC-Cy5, and CD8 PE-Cy7, and analyzed by flow cytometry. The CD45 marker allowed detection of the transferred CD45.2 T cells as the resident host T cells had the CD45.1 isoform. DEC-OVA + FGK vaccination induced a large expansion of OT-I cells, similar to prior reports (Bonifaz et al., 2002), while DEC-OVA FGK LPSiNP vaccination did not induce this expansion, and in fact seemed to have induced their deletion (Fig 13B-C).

8. Discussion

By displaying DEC-OVA and FGK together on nanoparticles, we aimed to simultaneously target antigen delivery and activation to the same APC, thus minimizing unnecessary inflammation that may occur when antigen and adjuvant are administered together, but as two separate entities. In addition, these particles might have produced a multivalent effect, in which the antibodies on the particle engaged multiple receptors on the cell. *In vitro* and short-term *in vivo* experiments showed that DEC-OVA nanoparticles targeted APCs effectively compared to HA-OVA nanoparticles. Unfortunately, the DEC-OVA nanoparticle was not sufficiently potent enough to generate T cell memory, and in fact, it seemed to induce deletion of antigen-specific T cells. Refinements to the nanoparticles, such as additional adjuvants like TLRs, altered ratios of components, or a different size particle may improve the efficacy of this approach as a vaccine. Conversely this approach could prove

useful to delete deleterious clones in autoimmune diseases for known antigenic specificities.

Figures

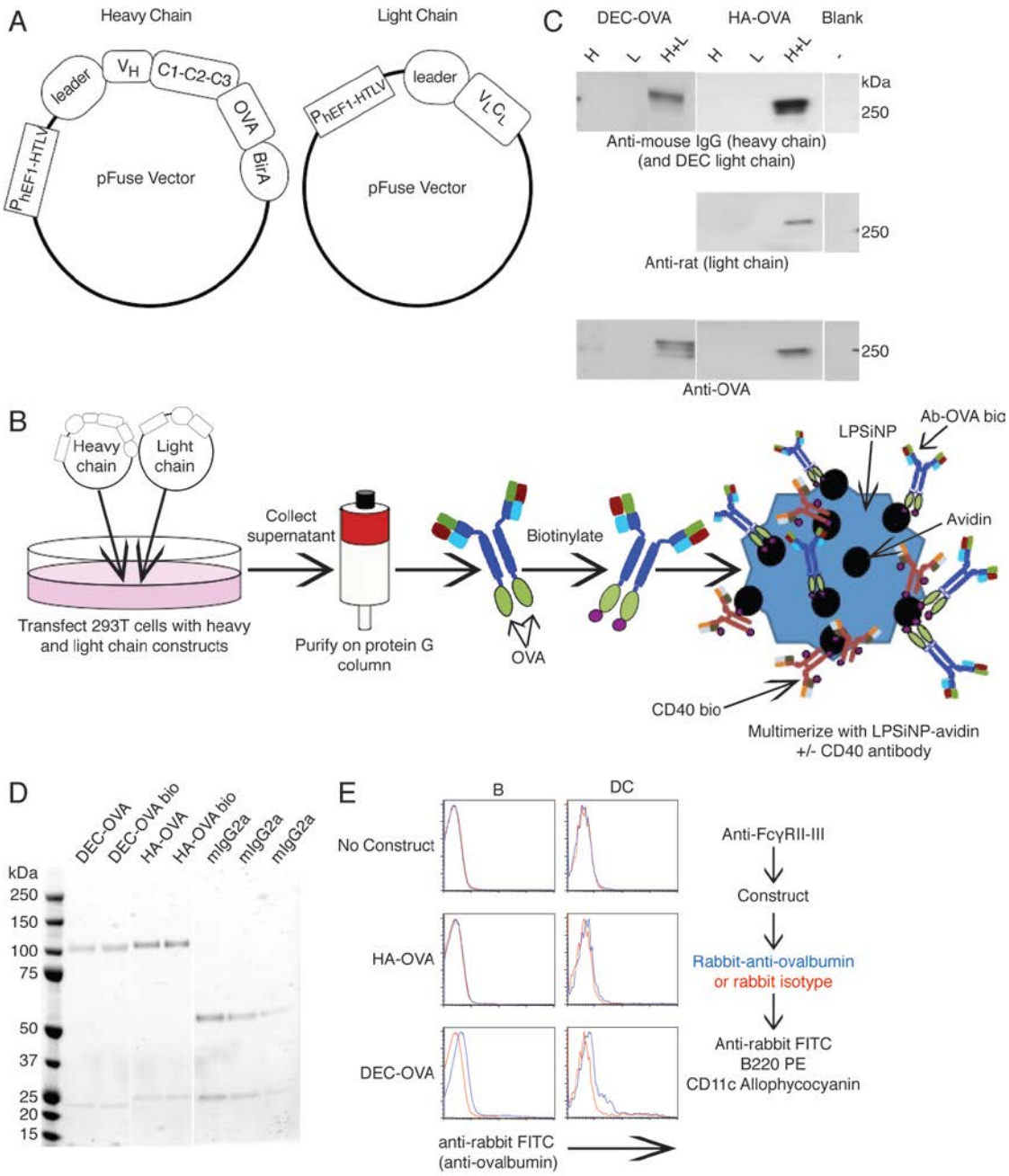

Figure 11. Antibody-OVA constructs. A) Plasmids used to generate HA-OVA construct. **B)** Schematic of protein expression, purification, and final LPSiNP configuration. **C)** Western for heavy chain, light chain, and OVA (non-reducing). **D)** Protein gel of constructs, and biotinylated constructs (non-reducing). **E)** B cell and DC staining with constructs.

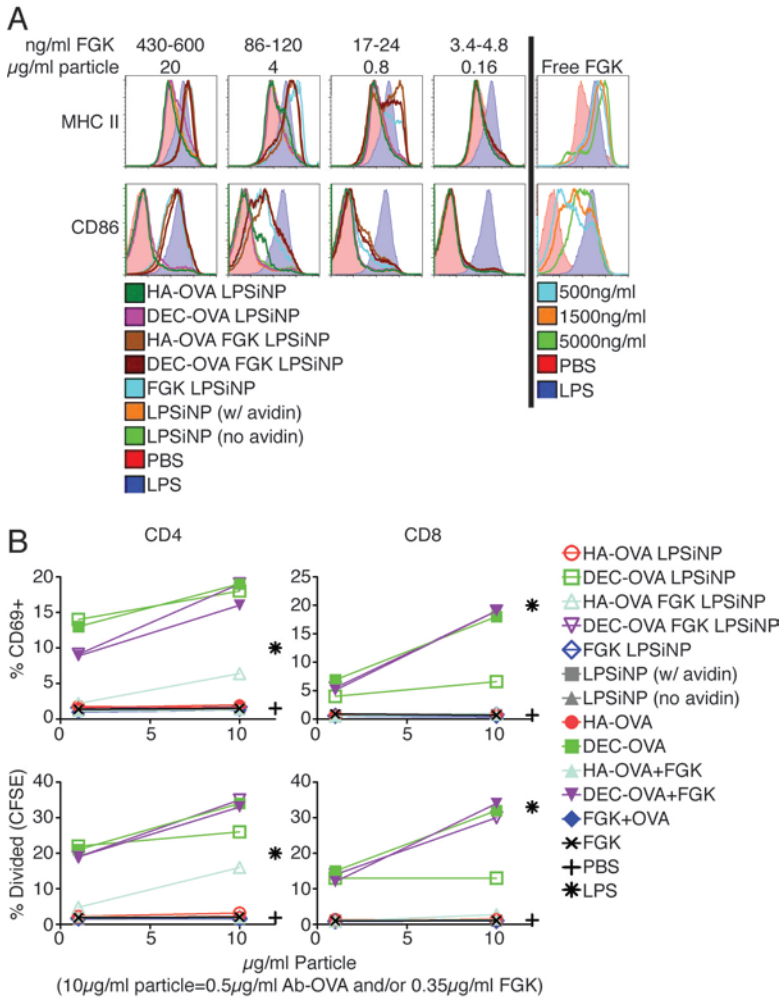

Figure 12. Antibody-OVA LPSiNP constructs *in vitro*. A) LPSiNPs were incubated with purified B cells from spleen for 2 days and analyzed by flow cytometry for their ability to upregulate CD86 and MHC II on B cells. **B)** LPSiNPs, antibody-OVAs ± FGK, or controls were incubated with BMDCs for 1 day, and then incubated with 250,000 CFSE-labeled OT-I (CD8) or OT-II (CD4) T cells for 2 days. Cells were stained for CD69, CD4, and CD8, and analyzed by flow cytometry for division (CFSE dilution) and upregulation of CD69 expression.

Figure 13. Antibody-OVA LPSiNP constructs *in vivo*. A) Short-term proliferation of antigen-specific cells is induced by DEC-OVA-containing LPSiNPs. 10^6 CFSE-labeled OT-I (CD8) T cells were given to CD45.1 mice i.v. and 1 day later, 1μg or 5μg LPSiNPs were given to mice s.c. in 1 hind footpad. Mice were sacrificed at day 3 and OT-I cells from popliteal (draining) LN, inguinal LN, and spleen were assessed by flow cytometry. Divided cells (CFSE dilution) and total transferred cell number are shown for each organ. **B-C.** Deletion of antigen-specific cells 2 weeks after injection of DEC-OVA-containing LPSiNPs. **B)** Cell transfer and injection were performed as in A (but cells were not CFSE-labeled). Mice were sacrificed at day 13 and assessed for total transferred cells by flow cytometry. **C)** Representative FACS plots.

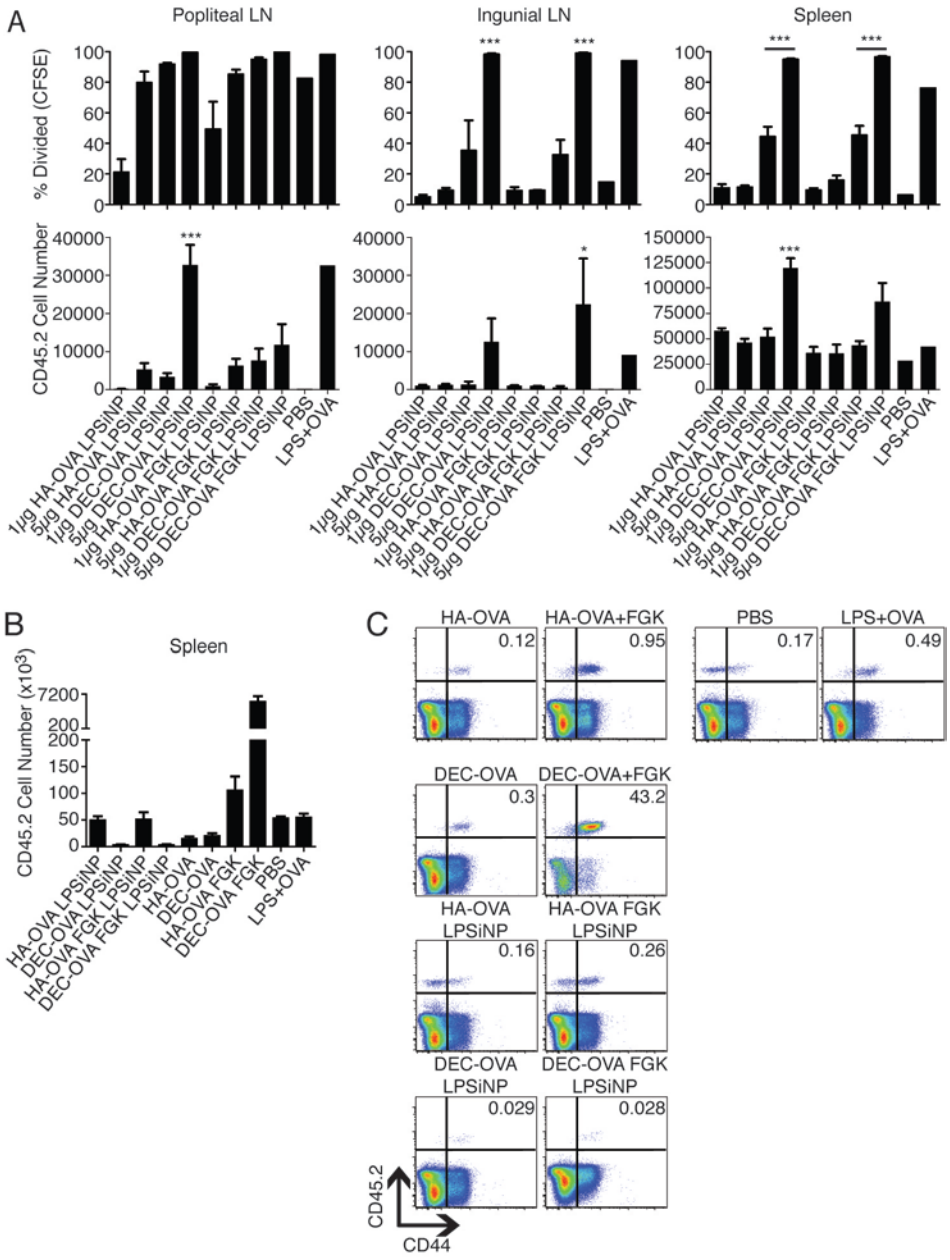
A
Popliteal LN
Ingunial LN
Spleen
% Divided (CFSE)
CD45.2 Cell Number
1μg HA-OVA LPSiNP
5μg HA-OVA LPSiNP
1μg DEC-OVA LPSiNP
5μg DEC-OVA LPSiNP
1μg HA-OVA FGK LPSiNP
5μg HA-OVA FGK LPSiNP
1μg DEC-OVA FGK LPSiNP
5μg DEC-OVA FGK LPSiNP
PBS
LPS+OVA
B
Spleen
CD45.2 Cell Number (x10³)
HA-OVA LPSiNP
DEC-OVA LPSiNP
HA-OVA FGK LPSiNP
DEC-OVA FGK LPSiNP
HA-OVA
DEC-OVA
HA-OVA FGK
DEC-OVA FGK
PBS
LPS+OVA
C
HA-OVA
HA-OVA+FGK
PBS
LPS+OVA
0.12
0.95
0.17
0.49
DEC-OVA
DEC-OVA+FGK
0.3
43.2
HA-OVA LPSiNP
HA-OVA FGK LPSiNP
0.16
0.26
DEC-OVA LPSiNP
DEC-OVA FGK LPSiNP
0.029
0.028
CD45.2
CD44

The Text of Chapter III, in part, has been submitted for publication. I was the secondary researcher and author, and the co-authors, Luo Gu, Zhengtao Qin, Maripat Corr, Stephen M. Hedrick, and Michael J. Sailor, directed and supervised the research which forms the basis for this chapter.

Chapter IV

Discussion

In these studies, we used particle-based vaccination to target APCs, deliver antigen, and deliver costimulation in a single package. We tested two particles, pH-sensitive hydrogel microparticles and luminescent porous silicon nanoparticles (LPSiNPs), for their ability to target APCs and induce a subsequent CD4 or CD8 T cell response. These particles varied in several aspects. The hydrogel microparticles were much bigger than the LPSiNPs (1.5μM vs 188nm) and they were immunostimulatory on their own, without adding FGK (anti-CD40) to the particle. Both particles could induce CD4 and CD8 responses *in vitro* and CD8 responses *in vivo* (at least in the short-term for LPSiNPs). CD4 responses may be induced *in vivo* by hydrogel microparticles, however, the OVA-specific CD4 response to VSV-OVA in blood was below the detectable limit of the assays and was not further explored. Both particles could induce upregulation of costimulatory markers on APCs *in vitro*, and hydrogel microparticles were also shown to induce this upregulation on DCs *in vivo*. LPSiNPs presented OVA on the surface of the particle, as part of an antibody-antigen hybrid protein, while hydrogel microparticles entrapped OVA in the particle. As the LPSiNPs seemed to be causing deletion of T cells, an antibody response was not tested for them. It was felt that the hydrogel microparticles would not be able to initiate a B cell response, as OVA was not present on the particle surface, and the particle would not hydrolyze until it reached the endosome.

One of the more interesting findings for the hydrogel microparticles was their recruitment of monocytes and neutrophils to the draining lymph node and their uptake by predominantly monocytes (greater than the amount of DCs that took them up). Particles in this size range generally have to be picked up by phagocytic cells and carried to the draining lymph node, as they are too big to migrate there themselves. Randolph et al. injected fluorescent microspheres into mice s.c. and found an influx of inflammatory monocytes to the site of injection, with 25% of those monocytes proceeding to the draining lymph node, where they expressed high levels of costimulatory markers and started expressing DC markers, becoming monocyte-derived DCs (moDCs; Randolph et al., 1999). We hypothesized that the monocytes taking up hydrogel microparticles in our system were also responding in this fashion. We did try to verify this, however, our attempts at showing that the moDCs were presenting antigen have been unsuccessful. The antibody which detects OT-I peptide (SIINFEKL) in the context of MHC H-2K^{b} (25-D1.16) could not detect differences *in vivo* in any condition (including positive control conditions). A magnetic bead purification kit for mouse monocytes does not exist, and our attempts at enriching for monocytes did not yield high enough purity. Thus, to isolate moDCs for use in an *in vitro* antigen presentation assay (i.e. ^{3}[H] proliferation assay), we will need to sort the cells via FACS. This experiment has not yet been done, and may require too many mice or particles to be feasible.

Particle-based vaccine delivery offered different advantages in these two systems. The hydrogel microparticles conferred immunostimulatory properties on the vaccine themselves, and targeting and/or activating antibodies did not improve the product. The LPSiNPs produced a multivalent effect of anti-CD40 compared to free antibody *in vitro* and a targeting effect *in vitro* and *in vivo*. However, they did not consistently produce long-lasting T cell responses, and it seemed they were not optimized for *in vivo* effects.

References

Ahonen, C.L., C.L. Doxsee, S.M. McGurran, T.R. Riter, W.F. Wade, R.J. Barth, J.P. Vasilakos, R.J. Noelle, and R.M. Kedl. 2004. Combined TLR and CD40 triggering induces potent CD8+ T cell expansion with variable dependence on type I IFN. *J Exp Med*. 199:775-784.

Ahonen, C.L., A. Wasiuk, S. Fuse, M.J. Turk, M.S. Ernstoff, A. a Suriawinata, J.D. Gorham, R.M. Kedl, E.J. Usherwood, and R.J. Noelle. 2008. Enhanced efficacy and reduced toxicity of multifactorial adjuvants compared with unitary adjuvants as cancer vaccines. *Blood*. 111:3116-3125.

Al-Daccak, R., N. Mooney, and D. Charron. 2004. MHC class II signaling in antigen-presenting cells. *Curr Opin Immunol*. 16:108-113.

Anderson, M.J., K. Shafer-Weaver, N.M. Greenberg, and A.A. Hurwitz. 2007. Tolerization of tumor-specific T cells despite efficient initial priming in a primary murine model of prostate cancer. *J Immunol*. 178:1268-1276.

Anderson, S.H.C., H. Elliott, D.J. Wallis, L.T. Canham, and J.J. Powell. 2003. Dissolution of different forms of partially porous silicon wafers under simulated physiological conditions. *Phys Status Solidi A*. 197:331-335.

Arvin, A.M. 2008. Humoral and cellular immunity to varicella-zoster virus: an overview. *J Infect Dis*. 197 Suppl:S58-60.

Ashley, C.E., E.C. Carnes, G.K. Phillips, D. Padilla, P.N. Durfee, P.A. Brown, T.N. Hanna, J. Liu, B. Phillips, M.B. Carter, N.J. Carroll, X. Jiang, D.R. Dunphy, C.L. Willman, D.N. Petsev, D.G. Evans, A.N. Parikh, B. Chackerian, W. Wharton, D.S. Peabody, and C.J. Brinker. 2011. The targeted delivery of multicomponent cargos to cancer cells by nanoporous particle-supported lipid bilayers. *Nat Mater*. 10:389-397.

Banchereau, J., F. Bazan, D. Blanchard, F. Briere, J.P. Galizzi, C. Vankooten, Y.J. Liu, F. Rousset, and S. Saeland. 1994. THE CD40 ANTIGEN AND ITS LIGAND. *Annu Rev Immunol*. 12:881-922.

Barr, T.A., A.L. McCormick, J. Carlring, and A.W. Heath. 2003. A potent adjuvant effect of CD40 antibody attached to antigen. *Immunology*. 109:87-92.

Beatty, G.L., E.G. Chiorean, M.P. Fishman, B. Saboury, U.R. Teitelbaum, W. Sun, R.D. Huhn, W. Song, D. Li, L.L. Sharp, D.A. Torigian, P.J. O'Dwyer, and R.H. Vonderheide. 2011. CD40 Agonists Alter Tumor Stroma and Show

Efficacy Against Pancreatic Carcinoma in Mice and Humans. *Science*. 331:1612-1616.

Becker, T., F.U. Hartl, and F. Wieland. 2002. CD40, an extracellular receptor for binding and uptake of Hsp70-peptide complexes. *J Cell Biol*. 158:1277-1285.

Bedoui, S., P.G. Whitney, J. Waithman, L. Eidsmo, L. Wakim, I. Caminschi, R.S. Allan, M. Wojtasiak, K. Shortman, F.R. Carbone, A.G. Brooks, and W.R. Heath. 2009. Cross-presentation of viral and self antigens by skin-derived CD103+ dendritic cells. *Nat Immunol*. 10:488-95.

Belz, G.T., C.M. Smith, L. Kleinert, P. Reading, A. Brooks, K. Shortman, F.R. Carbone, and W.R. Heath. 2004. Distinct migrating and nonmigrating dendritic cell populations are involved in MHC class I-restricted antigen presentation after lung infection with virus. *Proc Natl Acad Sci U.S.A.* 101:8670-5.

Bennett, S.R.M., F.R. Carbone, F. Karamalis, R.A. Flavell, J. Miller, and W.R. Heath. 1998. Help for cytotoxic-T-cell responses is mediated by CD40 signalling. *Nature*. 393:478-480.

Bennouna, S., and E.Y. Denkers. 2005. Microbial antigen triggers rapid mobilization of TNF-alpha to the surface of mouse neutrophils transforming them into inducers of high-level dendritic cell TNF-alpha production. *J Immunol*. 174:4845-51.

Berzofsky, J.A., J.D. Ahlers, and I.M. Belyakov. 2001. Strategies for designing and optimizing new generation vaccines. *Nat Rev Immunol*. 1:209-19.

Bevan, M.J. 1976. Cross-priming for a secondary cytotoxic response to minor H antigens with H-2 congenic cells which do not cross-react in the cytotoxic assay. *J Exp Med*. 143:1283-1288.

Bonifaz, L., D. Bonnyay, K. Mahnke, M. Rivera, M.C. Nussenzweig, and R.M. Steinman. 2002. Efficient Targeting of Protein Antigen to the Dendritic Cell Receptor DEC-205 in the Steady State Leads to Antigen Presentation on Major Histocompatibility Complex Class I Products and Peripheral CD8+ T Cell Tolerance. *J Exp Med*. 196:1627-1638.

Boyle, A.L., and D.N. Woolfson. 2011. De novo designed peptides for biological applications. *Chem Soc Rev*. 40:4295-306.

Brigger, I., C. Dubernet, and P. Couvreur. 2002. Nanoparticles in cancer therapy and diagnosis. *Adv Drug Deliver Rev*. 54:631-651.

Burgdorf, S., A. Kautz, V. Böhnert, P.A. Knolle, C. Kurts, and V. Bohnert. 2007. Distinct pathways of antigen uptake and intracellular routing in CD4 and CD8 T cell activation. *Science*. 316:612-6.

Burgdorf, S., C. Schölz, A. Kautz, R. Tampé, C. Kurts, C. Scholz, and R. Tampe. 2008. Spatial and mechanistic separation of cross-presentation and endogenous antigen presentation. *Nat Immunol*. 9:558-66.

Bursch, L.S., L. Wang, B. Igyarto, A. Kissenpfennig, B. Malissen, D.H. Kaplan, and K.A. Hogquist. 2007. Identification of a novel population of Langerin+ dendritic cells. *J Exp Med*. 204:3147-56.

Campbell, K.A., P.J. Ovendale, M.K. Kennedy, W.C. Fanslow, S.G. Reed, and C.R. Maliszewski. 1996. CD40 ligand is required for protective cell-mediated immunity to Leishmania major. *Immunity*. 4:283-289.

Canham, L.T. 1990. Silicon Quantum Wire Array Fabrication by Electrochemical and Chemical Dissolution of Wafers. *Appl Phys Lett*. 57:1046-1048.

Caramalho, I., T. Lopes-Carvalho, D. Ostler, S. Zelenay, M. Haury, and J. Demengeot. 2003. Regulatory T cells selectively express toll-like receptors and are activated by lipopolysaccharide. *J Exp Med*. 197:403-411.

Chen, J., L. Chen, G. Wang, and H. Tang. 2007. Cholesterol-dependent and -Independent CD40 internalization and signaling activation in cardiovascular endothelial cells. *Arterioscl Throm Vas*. 27:2005-2013.

Chen, Y., J. Chen, Y. Xiong, Q. Da, Y. Xu, X. Jiang, and H. Tang. 2006. Internalization of CD40 regulates its signal transduction in vascular endothelial cells. *Biochem Bioph Res Co*. 345:106-117.

Cheong, C., I. Matos, J.-H. Choi, D.B. Dandamudi, E. Shrestha, M.P. Longhi, K.L. Jeffrey, R.M. Anthony, C. Kluger, G. Nchinda, H. Koh, A. Rodriguez, J. Idoyaga, M. Pack, K. Velinzon, C.G. Park, and R.M. Steinman. 2010. Microbial stimulation fully differentiates monocytes to DC-SIGN/CD209(+) dendritic cells for immune T cell areas. *Cell*. 143:416-29.

Cho, N.-H., T.-C. Cheong, J.H. Min, J.H. Wu, S.J. Lee, D. Kim, J.-S. Yang, S. Kim, Y.K. Kim, and S.-Y. Seong. 2011. A multifunctional core-shell nanoparticle for dendritic cell-based cancer immunotherapy. *Nature Nanotechnol*. 6:675-682.

Choi, H.S., W. Liu, P. Misra, E. Tanaka, J.P. Zimmer, B. Itty Ipe, M.G. Bawendi, and J.V. Frangioni. 2007. Renal clearance of quantum dots. *Nature Biotechnol*. 25:1165-70.

Chorro, L., A. Sarde, M. Li, K.J. Woollard, P. Chambon, B. Malissen, A. Kissenpfennig, J.-B. Barbaroux, R. Groves, and F. Geissmann. 2009. Langerhans cell (LC) proliferation mediates neonatal development, homeostasis, and inflammation-associated expansion of the epidermal LC network. *J Exp Med*. 206:3089-100.

Copland, M.J., T. Rades, N.M. Davies, and M.A. Baird. 2005. Lipid based particulate formulations for the delivery of antigen. *Immunol Cell Biol*. 83:97-105.

Crawford, A., M. Macleod, T. Schumacher, L. Corlett, and D. Gray. 2006. Primary T cell expansion and differentiation in vivo requires antigen presentation by B cells. *J Immunol*. 176:3498-506.

Cui, Z., S.-J. Han, D.P. Vangasseri, and L. Huang. 2005. Immunostimulation mechanism of LPD nanoparticle as a vaccine carrier. *Mol Pharm*. 2:22-28.

Curtsinger, J.M., M.Y. Gerner, D.C. Lins, and M.F. Mescher. 2007. Signal 3 availability limits the CD8 T cell response to a solid tumor. *J Immunol*. 178:6752-6760.

Dejean, A.S., D.R. Beisner, I.L. Ch'en, Y.M. Kerdiles, A. Babour, K.C. Arden, D.H. Castrillon, R.A. DePinho, and S.M. Hedrick. 2009. Transcription factor Foxo3 controls the magnitude of T cell immune responses by modulating the function of dendritic cells. *Nat Immunol*. 10:504-13.

Demento, S.L., S.C. Eisenbarth, H.G. Foellmer, C. Platt, M.J. Caplan, W.M. Saltzman, I. Mellman, M. Ledizet, E. Fikrig, R.A. Flavell, T.M. Fahmy, and W. Mark Saltzman. 2009. Inflammasome-activating nanoparticles as modular systems for optimizing vaccine efficacy. *Vaccine*. 27:3013-3021.

DiPucchio, T., B. Chatterjee, A. Smed-Sörensen, S. Clayton, A. Palazzo, M. Montes, Y. Xue, I. Mellman, J. Banchereau, J.E. Connolly, and A. Smed-Sorensen. 2008. Direct proteasome-independent cross-presentation of viral antigen by plasmacytoid dendritic cells on major histocompatibility complex class I. *Nat Immunol*. 9:551-7.

Diwan, M., P. Elamanchili, H. Lane, A. Gainer, and J. Samuel. 2003. Biodegradable nanoparticle mediated antigen delivery to human cord blood

derived dendritic cells for induction of primary T cell responses. *J Drug Target*. 11:495-507.

Dobrovolskaia, M.A., and S.E. McNeil. 2007. Immunological properties of engineered nanomaterials. *Nature Nanotechnol*. 2:469-478.

Dougan, M., and G. Dranoff. 2009. Immune Therapy for Cancer. *In* Annu Rev Immunol. 83-117.

Dudziak, D., A.O. Kamphorst, G.F. Heidkamp, V.R. Buchholz, C. Trumpfheller, S. Yamazaki, C. Cheong, K. Liu, H.-W.W. Lee, C.G. Park, R.M. Steinman, and M.C. Nussenzweig. 2007. Differential antigen processing by dendritic cell subsets in vivo. *Science*. 315:107-111.

Van Dyck, K., H. Robberecht, R. Van Cauwenbergh, V. Van Vlaslaer, and H. Deelstra. 2000. Indication of silicon essentiality in humans - Serum concentrations in Belgian children and adults, including pregnant women. *Biol Trace Elem Res*. 77:25-32.

Elamanchili, P., M. Diwan, M. Cao, and J. Samuel. 2004. Characterization of poly(D,L-lactic-co-glycolic acid) based nanoparticulate system for enhanced delivery of antigens to dendritic cells. *Vaccine*. 22:2406-2412.

Erogbogbo, F., K.-T. Yong, I. Roy, G. Xu, P.N. Prasad, and M.T. Swihart. 2008. Biocompatible luminescent silicon quantum dots for imaging of cancer cells. *ACS Nano*. 2:873-878.

Frleta, D., D. Demian, and W.F. Wade. 2001. Class II-targeted antigen is superior to CD40-targeted antigen at stimulating humoral responses in vivo. *Int Immunopharmacol*. 1:265-75.

Gao, X.H., Y.Y. Cui, R.M. Levenson, L.W.K. Chung, and S.M. Nie. 2004. In vivo cancer targeting and imaging with semiconductor quantum dots. *Nature Biotechnol*. 22:969-976.

Garcia-Sastre, A., and C.A. Biron. 2006. Type 1 interferons and the virus-host relationship: a lesson in detente. *Science*. 312:879-882.

Geissmann, F., S. Jung, and D.R. Littman. 2003. Blood monocytes consist of two principal subsets with distinct migratory properties. *Immunity*. 19:71-82.

Gerner, M.Y., K.A. Casey, and M.F. Mescher. 2008. Defective MHC class II presentation by dendritic cells limits CD4 T cell help for antitumor CD8 T cell responses. *J Immunol*. 181:155-164.

Gerosa, F., B. Baldani-Guerra, L.A. Lyakh, G. Batoni, S. Esin, R.T. Winkler-Pickett, M.R. Consolaro, M. De Marchi, D. Giachino, A. Robbiano, M. Astegiano, A. Sambataro, R.A. Kastelein, G. Carra, and G. Trinchieri. 2008. Differential regulation of interleukin 12 and interleukin 23 production in human dendritic cells. *J Exp Med*. 205:1447-1461.

Ginhoux, F., M.P. Collin, M. Bogunovic, M. Abel, M. Leboeuf, J. Helft, J. Ochando, A. Kissenpfennig, B. Malissen, M. Grisotto, H. Snoeck, G. Randolph, and M. Merad. 2007. Blood-derived dermal langerin+ dendritic cells survey the skin in the steady state. *J Exp Med*. 204:3133-46.

van Gisbergen, K.P.J.M., I.S. Ludwig, T.B.H. Geijtenbeek, and Y. van Kooyk. 2005a. Interactions of DC-SIGN with Mac-1 and CEACAM1 regulate contact between dendritic cells and neutrophils. *FEBS Lett*. 579:6159-68.

van Gisbergen, K.P.J.M., M. Sanchez-Hernandez, T.B.H. Geijtenbeek, and Y. van Kooyk. 2005b. Neutrophils mediate immune modulation of dendritic cells through glycosylation-dependent interactions between Mac-1 and DC-SIGN. *J Exp Med*. 201:1281-92.

Gu, L., J.-H. Park, K.H. Duong, E. Ruoslahti, and M.J. Sailor. 2010. Magnetic Luminescent Porous Silicon Microparticles for Localized Delivery of Molecular Drug Payloads. *Small*. 6:2546-2552.

den Haan, J.M.M., S.M. Lehar, and M.J. Bevan. 2000. Cd8+ but Not Cd8- Dendritic Cells Cross-Prime Cytotoxic T Cells in Vivo. *J Exp Med*. 192:1685-1696.

Hawiger, D., K. Inaba, Y. Dorsett, M. Guo, K. Mahnke, M. Rivera, J.V. Ravetch, R.M. Steinman, and M.C. Nussenzweig. 2001. Dendritic cells induce peripheral T cell unresponsiveness under steady state conditions in vivo. *J Exp Med*. 194:769-779.

Hayashi, F., K.D. Smith, A. Ozinsky, T.R. Hawn, E.C. Yi, D.R. Goodlett, J.K. Eng, S. Akira, D.M. Underhill, and A. Aderem. 2001. The innate immune response to bacterial flagellin is mediated by Toll-like receptor 5. *Nature*. 410:1099-103.

Hedrick, S.M., and R.H. Schwartz. 1983. The T cell response to allelic determinants on Igh-1-encoded IgG2a antibodies: dual recognition examined by using antigenic antibodies with binding affinity for Ia molecules. *J Immunol*. 130:1958-66.

Heinrich, J.L., C.L. Curtis, G.M. Credo, K.L. Kavanagh, and M.J. Sailor. 1992. Luminescent Colloidal Silicon Suspensions From Porous Silicon. *Science*. 255:66-68.

Hemmi, H., O. Takeuchi, T. Kawai, T. Kaisho, S. Sato, H. Sanjo, M. Matsumoto, K. Hoshino, H. Wagner, K. Takeda, and S. Akira. 2000. A Toll-like receptor recognizes bacterial DNA. *Nature*. 408:740-5.

Hodi, F.S., S.J. O'Day, D.F. McDermott, R.W. Weber, J.A. Sosman, J.B. Haanen, R. Gonzalez, C. Robert, D. Schadendorf, J.C. Hassel, W. Akerley, A.J.M. van den Eertwegh, J. Lutzky, P. Lorigan, J.M. Vaubel, G.P. Linette, D. Hogg, C.H. Ottensmeier, C. Lebbe, C. Peschel, I. Quirt, J.I. Clark, J.D. Wolchok, J.S. Weber, J. Tian, M.J. Yellin, G.M. Nichol, A. Hoos, and W.J. Urba. 2010. Improved Survival with Ipilimumab in Patients with Metastatic Melanoma. *N Engl J Med*. 363:711-723.

Hoft, D.F. 2008. Tuberculosis vaccine development: goals, immunological design, and evaluation. *Lancet*. 372:164-75.

Hong, S., P.R. Leroueil, I.J. Majoros, B.G. Orr, J.R. Baker Jr., and M.M.B. Holl. 2007. The binding avidity of a nanoparticle-based multivalent targeted drug delivery platform. *Chem Biol*. 14:107-115.

Hunder, N.N., H. Wallen, J. Cao, D.W. Hendricks, J.Z. Reilly, R. Rodmyre, A. Jungbluth, S. Gnjatic, J.A. Thompson, and C. Yee. 2008. Treatment of metastatic melanoma with autologous CD4+T cells against NY-ESO-1. *N Engl J Med*. 358:2698-2703.

Jackaman, C., S. Cornwall, P.T. Graham, and D.J. Nelson. 2011. CD40-activated B cells contribute to mesothelioma tumor regression. *Immunol Cell Biol*. 89:255-267.

Jain, R., S.M. Standley, and J.M.J. Fréchet. 2007. Synthesis and Degradation of pH-Sensitive Linear Poly(amidoamine)s. *Macromolecules*. 40:452-457.

Janeway, C.A. 1989. Approaching the asymptote? Evolution and revolution in immunology. *Cold Spring Harb Symp Quant Biol*. 54 Pt 1:1-13.

Jung, S., D. Unutmaz, P. Wong, G. Sano, K. De los Santos, T. Sparwasser, S. Wu, S. Vuthoori, K. Ko, F. Zavala, E.G. Pamer, D.R. Littman, and R.A. Lang. 2002. In vivo depletion of CD11c(+) dendritic cells abrogates priming of CD8(+) T cells by exogenous cell-associated antigens. *Immunity*. 17:211-220.

Kamanaka, M., P. Yu, T. Yasui, K. Yoshida, T. Kawabe, T. Horii, T. Kishimoto, and H. Kikutani. 1996. Protective role of CD40 in Leishmania major infection at two distinct phases of cell-mediated immunity. *Immunity*. 4:275-281.

Kantoff, P.W., C.S. Higano, N.D. Shore, E.R. Berger, E.J. Small, D.F. Penson, C.H. Redfern, A.C. Ferrari, R. Dreicer, R.B. Sims, Y. Xu, M.W. Frohlich, P.F. Schellhammer, T. Ahmed, A. Amin, J. Arseneau, N. Barth, G. Bernstein, B. Bracken, P. Burch, V. Caggiano, J. Chin, G. Chodak, F. Chu, J. Corman, B. Curti, N. Dawson, J.F. Deeken, T. Dubernet, M. Fishman, R. Flanigan, F. Gailani, L. Garbo, T. Gardner, E. Gelmann, D. George, T. Godfrey, L. Gomella, M. Guerra, S. Hall, J. Hanson, R. Israeli, E. Jancis, M.A.S. Jewett, V. Kassabian, J. Katz, L. Klotz, K. Koeneman, H. Koh, R. Kratzke, R. Lance, J. Lech, L. Leichman, R. Lemon, J. Liang, J. Libertino, M. Lilly, I. Malik, S.E. Martin, J. McCaffrey, D. McLeod, D. McNeel, B. Miles, M. Murdock, C. Nabhan, J. Nemunaitis, D. Notter, A. Pantuck, P. Perrotte, D. Pessis, D. Petrylak, J. Polikoff, P. Pommerville, S. Ramanathan, M. Rarick, J. Richards, R. Rifkin, N. Rohatgi, R. Rosenbluth, R. Santucci, A. Sayegh, J. Seigne, I. Shapira, N. Shedhadeh, D. Shepherd, S. Sridhar, R. Stephenson, C. Teigland, N. Thaker, J. Vacirca, L. Villa Jr., N. Vogelzang, M. Wertheim, J.H. Wolff, R. Wurzel, C. Yang, J. Young, and I.S. Investigators. 2010. Sipuleucel-T Immunotherapy for Castration-Resistant Prostate Cancer. *N Engl J Med*. 363:411-422.

Kasturi, S.P., I. Skountzou, R. a Albrecht, D. Koutsonanos, T. Hua, H.I. Nakaya, R. Ravindran, S. Stewart, M. Alam, M. Kwissa, F. Villinger, N. Murthy, J. Steel, J. Jacob, R.J. Hogan, A. García-Sastre, R. Compans, and B. Pulendran. 2011. Programming the magnitude and persistence of antibody responses with innate immunity. *Nature*. 470:543-7.

Klippstein, R., and D. Pozo. 2010. Nanotechnology-based manipulation of dendritic cells for enhanced immunotherapy strategies. *Nanomed-Nanotechnol*. 6:523-529.

Kwon, Y.J., E. James, N. Shastri, and J.M.J. Fréchet. 2005a. In vivo targeting of dendritic cells for activation of cellular immunity using vaccine carriers based on pH-responsive microparticles. *Proc Natl Acad Sci U.S.A.* 102:18264-8.

Kwon, Y.J., S.M. Standley, S.L. Goh, and J.M.J. Fréchet. 2005b. Enhanced antigen presentation and immunostimulation of dendritic cells using acid-degradable cationic nanoparticles. *J Control Release*. 105:199-212.

Lee, C., H. Kim, Y. Cho, and W.I. Lee. 2007. The properties of porous silicon as a therapeutic agent via the new photodynamic therapy. *J Mater Chem*. 17:2648.

Lee, S.J., S. Evers, D. Roeder, A.F. Parlow, J. Risteli, L. Risteli, Y.C. Lee, T. Feizi, H. Langen, and M.C. Nussenzweig. 2002. Mannose receptor-mediated regulation of serum glycoprotein homeostasis. *Science*. 295:1898-1901.

Lehmann, V., and U. Gosele. 1991. Porous Silicon Formation--A Quantum Wire Effect. *Appl Phys Lett*. 58:856-858.

Levin, M.J., M.N. Oxman, J.H. Zhang, G.R. Johnson, H. Stanley, A.R. Hayward, M.J. Caulfield, M.R. Irwin, J.G. Smith, J. Clair, I.S.F. Chan, H. Williams, R. Harbecke, R. Marchese, S.E. Straus, A. Gershon, and A. Weinberg. 2008. Varicella-zoster virus-specific immune responses in elderly recipients of a herpes zoster vaccine. *J Infect Dis*. 197:825-35.

León, B., M. López-Bravo, and C. Ardavín. 2007. Monocyte-derived dendritic cells formed at the infection site control the induction of protective T helper 1 responses against Leishmania. *Immunity*. 26:519-31.

Li, A., L. Qin, D. Zhu, R. Zhu, J. Sun, and S. Wang. 2010. Signalling pathways involved in the activation of dendritic cells by layered double hydroxide nanoparticles. *Biomaterials*. 31:748-756.

Li, F., and J.V. Ravetch. 2011. Inhibitory Fc gamma Receptor Engagement Drives Adjuvant and Anti-Tumor Activities of Agonistic CD40 Antibodies. *Science*. 333:1030-1034.

Li, H., Y. Li, J. Jiao, and H.-M. Hu. 2011. Alpha-alumina nanoparticles induce efficient autophagy-dependent cross-presentation and potent antitumour response. *Nature Nanotechnol*. 6:645-650.

Liu, Z., W. Cai, L. He, N. Nakayama, K. Chen, X. Sun, X. Chen, and H. Dai. 2007. In vivo biodistribution and highly efficient tumour targeting of carbon nanotubes in mice. *Nature Nanotechnol*. 2:47-52.

Low, S.P., N.H. Voelcker, L.T. Canham, and K.A. Williams. 2009. The biocompatibility of porous silicon in tissues of the eye. *Biomaterials*. 30:2873-2880.

Lyman, M.A., S. Aung, J.A. Biggs, and L.A. Sherman. 2004. A spontaneously arising pancreatic tumor does not promote the differentiation of naive CD8+ T lymphocytes into effector CTL. *J Immunol*. 172:6558-6567.

Makidon, P.E., A.U. Bielinska, S.S. Nigavekar, K.W. Janczak, J. Knowlton, A.J. Scott, N. Mank, Z.Y. Cao, S. Rathinavelu, M.R. Beer, J.E. Wilkinson, L.P. Blanco, J.J. Landers, and J.R. Baker. 2008. Pre-Clinical Evaluation of a Novel Nanoemulsion-Based Hepatitis B Mucosal Vaccine. *Plos One*. 3.

Makidon, P.E., J. Knowlton, J.V. Groom, L.P. Blanco, J.J. LiPuma, A.U. Bielinska, and J.R. Baker. 2010. Induction of immune response to the 17 kDa OMPA Burkholderia cenocepacia polypeptide and protection against pulmonary infection in mice after nasal vaccination with an OMP nanoemulsion-based vaccine. *Med Microbiol Immun*. 199:81-92.

Mauri, C., L.T. Mars, and M. Londei. 2000. Therapeutic activity of agonistic monoclonal antibodies against CD40 in a chronic autoimmune inflammatory process. *Nat Med*. 6:673-679.

McElhaney, J.E., D. Xie, W.D. Hager, M.B. Barry, Y. Wang, A. Kleppinger, C. Ewen, K.P. Kane, and R.C. Bleackley. 2006. T cell responses are better correlates of vaccine protection in the elderly. *J Immunol*. 176:6333-9.

Megiovanni, A.M., F. Sanchez, M. Robledo-Sarmiento, C. Morel, J.C. Gluckman, and S. Boudaly. 2006. Polymorphonuclear neutrophils deliver activation signals and antigenic molecules to dendritic cells: a new link between leukocytes upstream of T lymphocytes. *J Leukoc Biol*. 79:977-88.

Moghimi, S.M., A.C. Hunter, and J.C. Murray. 2001. Long-circulating and target-specific nanoparticles: Theory to practice. *Pharmacol Rev*. 53:283-318.

Montet, X., M. Funovics, K. Montet-Abou, R. Weissleder, and L. Josephson. 2006. Multivalent effects of RGD peptides obtained by nanoparticle display. *J Med Chem*. 49:6087-6093.

Moon, J.J., H. Suh, A. Bershteyn, M.T. Stephan, H. Liu, B. Huang, M. Sohail, S. Luo, S.H. Um, H. Khant, J.T. Goodwin, J. Ramos, W. Chiu, and D.J. Irvine. 2011. Interbilayer-crosslinked multilamellar vesicles as synthetic vaccines for potent humoral and cellular immune responses. *Nat Mater*. 10:243-251.

Moore, M.W., F.R. Carbone, and M.J. Bevan. 1988. Introduction of soluble protein into the class I pathway of antigen processing and presentation. *Cell*. 54:777-85.

Mouries, J., G. Moron, G. Schlecht, N. Escriou, G. Dadaglio, and C. Leclerc. 2008. Plasmacytoid dendritic cells efficiently cross-prime naive T cells in vivo after TLR activation. *Blood*. 112:3713-3722.

Mundargi, R.C., V.R. Babu, V. Rangaswamy, P. Patel, and T.M. Aminabhavi. 2008. Nano/micro technologies for delivering macromolecular therapeutics using poly(D,L-lactide-co-glycolide) and its derivatives. *J Control Release*. 125:193-209.

Murthy, N., Y.X. Thng, S. Schuck, M.C. Xu, and J.M.J. Fréchet. 2002. A novel strategy for encapsulation and release of proteins: hydrogels and microgels with acid-labile acetal cross-linkers. *J Am Chem Soc*. 124:12398-9.

Murthy, N., M. Xu, S. Schuck, J. Kunisawa, N. Shastri, and J.M.J. Fréchet. 2003. A macromolecular delivery vehicle for protein-based vaccines: acid-degradable protein-loaded microgels. *Proc Natl Acad Sci U.S.A.* 100:4995-5000.

Okada, C.Y., and M. Rechsteiner. 1982. Introduction of macromolecules into cultured mammalian cells by osmotic lysis of pinocytic vesicles. *Cell*. 29:33-41.

Palm, N.W., and R. Medzhitov. 2009. Pattern recognition receptors and control of adaptive immunity. *Immunol Rev*. 227:221-33.

Palucka, K., J. Banchereau, and I. Mellman. 2010. Designing Vaccines Based on Biology of Human Dendritic Cell Subsets. *Immunity*. 33:464-478.

Paramonov, S.E., E.M. Bachelder, T.T. Beaudette, S.M. Standley, C.C. Lee, J. Dashe, and J.M.J. Fréchet. 2008. Fully acid-degradable biocompatible polyacetal microparticles for drug delivery. *Bioconj Chem*. 19:911-9.

Pardoll, D.M. 2002. Spinning molecular immunology into successful immunotherapy. *Nat Rev Immunol*. 2:227-238.

Park, J.-H., G. von Maltzahn, L. Zhang, A.M. Derfus, D. Simberg, T.J. Harris, E. Ruoslahti, S.N. Bhatia, and M.J. Sailor. 2009a. Systematic Surface Engineering of Magnetic Nanoworms for in vivo Tumor Targeting. *Small*. 5:694-700.

Park, J.-ho, L. Gu, G. von Maltzahn, E. Ruoslahti, S.N. Bhatia, M.J. Sailor, and G.V. Maltzahn. 2009b. Biodegradable luminescent porous silicon nanoparticles for in vivo applications. *Nat Mater*. 8:331-336.

Pathak, S.S., J.D. Lich, and J.S. Blum. 2001. Cutting edge: editing of recycling class II:peptide complexes by HLA-DM. *J Immunol*. 167:632-635.

Peek, L.J., C.R. Middaugh, and C. Berkland. 2008. Nanotechnology in vaccine delivery. *Adv Drug Deliver Rev*. 60:915-928.

Peer, D., J.M. Karp, S. Hong, O.C. FaroKhzad, R. Margalit, and R. Langer. 2007. Nanocarriers as an emerging platform for cancer therapy. *Nature Nanotechnol*. 2:751-760.

Petersen, L.K., L. Xue, M.J. Wannemuehler, K. Rajan, and B. Narasimhan. 2009. The simultaneous effect of polymer chemistry and device geometry on the in vitro activation of murine dendritic cells. *Biomaterials*. 30:5131-5142.

Popplewell, J.F., S.J. King, J.P. Day, P. Ackrill, L.K. Fifield, R.G. Cresswell, M.L. di Tada, and K. Liu. 1998. Kinetics of uptake and elimination of silicic acid by a human subject: a novel application of 32Si and accelerator mass spectrometry. *J Inorg Biochem*. 69:177-80.

Porter, D.L., B.L. Levine, M. Kalos, A. Bagg, and C.H. June. 2011. Chimeric Antigen Receptor-Modified T Cells in Chronic Lymphoid Leukemia. *N Engl J Med*. 365:725-733.

Poulin, L.F., S. Henri, B. de Bovis, E. Devilard, A. Kissenpfennig, and B. Malissen. 2007. The dermis contains langerin+ dendritic cells that develop and function independently of epidermal Langerhans cells. *J Exp Med*. 204:3119-31.

Pulendran, B., and R. Ahmed. 2011. Immunological mechanisms of vaccination. *Nat Immunol*. 131:509-17.

Randolph, G.J., K. Inaba, D.F. Robbiani, R.M. Steinman, and W.A. Muller. 1999. Differentiation of phagocytic monocytes into lymph node dendritic cells in vivo. *Immunity*. 11:753-61.

Reddy, S.T., A.J. van der Vlies, E. Simeoni, V. Angeli, G.J. Randolph, C.P. O'Neill, L.K. Lee, M.A. Swartz, and J.A. Hubbell. 2007. Exploiting lymphatic transport and complement activation in nanoparticle vaccines. *Nature Biotechnol*. 25:1159-1164.

Rodríguez-Pinto, D., and J. Moreno. 2005. B cells can prime naive CD4+ T cells in vivo in the absence of other professional antigen-presenting cells in a CD154-CD40-dependent manner. *Eur J Immunol*. 35:1097-105.

Rolink, A., F. Melchers, and J. Andersson. 1996. The SCID but not the RAG-2 gene product is required for S mu-S epsilon heavy chain class switching. *Immunity*. 5:319-30.

Ron, Y., and J. Sprent. 1987. T cell priming in vivo: a major role for B cells in presenting antigen to T cells in lymph nodes. *J Immunol*. 138:2848-56.

Rosenberg, S.A., J.C. Yang, and N.P. Restifo. 2004. Cancer immunotherapy: moving beyond current vaccines. *Nat Med*. 10:909-915.

Ruoslahti, E., S.N. Bhatia, and M.J. Sailor. 2010. Targeting of drugs and nanoparticles to tumors. *J Cell Biol*. 188:759-768.

Sailor, M.J. 2012. Porous Silicon in Practice: Preparation, Characterization, and Applications. Wiley-VCH, Weinheim, Germany.

Salonen, J., L. Laitinen, A.M. Kaukonen, J. Tuura, M. Bjorkqvist, T. Heikkila, K. Vaha-Heikkila, J. Hirvonen, and V.P. Lehto. 2005. Mesoporous silicon microparticles for oral drug delivery: Loading and release of five model drugs. *J Control Release*. 108:362-374.

Sassi, A.P., A.J. Shaw, H.W. Blanch, and J.M. Prausnitz. 1996. Partitioning of proteins and small biomolecules in temperature- and pH-sensitive hydrogels. *Polymer*. 37:2151-2164.

Schoenberger, S.P., R.E.M. Toes, E.I.H. van der Voort, R. Offringa, and C.J.M. Melief. 1998. T-cell help for cytotoxic T lymphocytes is mediated by CD40-CD40L interactions. *Nature*. 393:480-483.

Serbina, N.V., and E.G. Pamer. 2006. Monocyte emigration from bone marrow during bacterial infection requires signals mediated by chemokine receptor CCR2. *Nat Immunol*. 7:311-317.

Serda, R.E., J. Go, R.C. Bhavane, X. Liu, C. Chiappini, P. Decuzzi, and M. Ferrari. 2009. The association of silicon microparticles with endothelial cells in drug delivery to the vasculature. *Biomaterials*. 30:2440-2448.

Shen, H., A.L. Ackerman, V. Cody, A. Giodini, E.R. Hinson, P. Cresswell, R.L. Edelson, W.M. Saltzman, and D.J. Hanlon. 2006. Enhanced and prolonged cross-presentation following endosomal escape of exogenous antigens encapsulated in biodegradable nanoparticles. *Immunology*. 117:78-88.

Shklovskaya, E., B.J. O'Sullivan, L.G. Ng, B. Roediger, R. Thomas, W. Weninger, and B. Fazekas de St Groth. 2011. Langerhans cells are precommitted to immune tolerance induction. *Proc Natl Acad Sci U.S.A.* 108:18049-54.

Shrimpton, R.E., M. Butler, A.-S.S. Morel, E. Eren, S.S. Hue, and M.A. Ritter. 2009. CD205 (DEC-205): a recognition receptor for apoptotic and necrotic self. *Mol Immunol*. 46:1229-1239.

Sinnathamby, G., and L.C. Eisenlohr. 2003. Presentation by recycling MHC class II molecules of an influenza hemagglutinin-derived epitope that is revealed in the early endosome by acidification. *J Immunol*. 170:3504-3513.

Skea, D.L., and B.H. Barber. 1993. Studies of the adjuvant-independent antibody response to immunotargeting. Target structure dependence, isotype distribution, and induction of long term memory. *J Immunol*. 151:3557-3568.

Slowing, I., B.G. Trewyn, and V.S.Y. Lin. 2006. Effect of surface functionalization of MCM-41-type mesoporous silica nanoparticleson the endocytosis by human cancer cells. *J Am Chem Soc*. 128:14792-14793.

Slutter, B., P.C. Soema, Z. Ding, R. Verheul, W. Hennink, and W. Jiskoot. 2010. Conjugation of ovalbumin to trimethyl chitosan improves immunogenicity of the antigen. *J Control Release*. 143:207-214.

Soong, L., J.C. Xu, I.S. Grewal, P. Kima, J. Sun, B.J. Longley Jr., N.H. Ruddle, D. McMahon-Pratt, and R.A. Flavell. 1996. Disruption of CD40-CD40 ligand interactions results in an enhanced susceptibility to Leishmania amazonensis infection. *Immunity*. 4:263-273.

Standley, S.M., Y.J. Kwon, N. Murthy, J. Kunisawa, N. Shastri, S.J. Guillaudeu, L. Lau, and J.M.J. Fréchet. 2004. Acid-degradable particles for protein-based vaccines: enhanced survival rate for tumor-challenged mice using ovalbumin model. *Bioconj Chem*. 15:1281-8.

Standley, S.M., I. Mende, S.L. Goh, Y.J. Kwon, T.T. Beaudette, E.G. Engleman, and J.M.J. Fréchet. 2007. Incorporation of CpG oligonucleotide ligand into protein-loaded particle vaccines promotes antigen-specific CD8 T-cell immunity. *Bioconj Chem*. 18:77-83.

Tasciotti, E., X. Liu, R. Bhavane, K. Plant, A.D. Leonard, B.K. Price, M.M.-C. Cheng, P. Decuzzi, J.M. Tour, F. Robertson, and M. Ferrari. 2008. Mesoporous silicon particles as a multistage delivery system for imaging and therapeutic applications. *Nature Nanotechnol*. 3:151-157.

Uto, T., X. Wang, K. Sato, M. Haraguchi, T. Akagi, M. Akashi, and M. Baba. 2007. Targeting of antigen to dendritic cells with poly(gamma-glutamic acid) nanoparticles induces antigen-specific humoral and cellular immunity. *J Immunol*. 178:2979-2986.

Varol, C., L. Landsman, D.K. Fogg, L. Greenshtein, B. Gildor, R. Margalit, V. Kalchenko, F. Geissmann, and S. Jung. 2007. Monocytes give rise to mucosal, but not splenic, conventional dendritic cells. *J Exp Med*. 204:171-80.

Vonderheide, R.H., K.T. Flaherty, M. Khalil, M.S. Stumacher, D.L. Bajor, N.A. Hutnick, P. Sullivan, J.J. Mahany, M. Gallagher, A. Kramer, S.J. Green, P.J. O'Dwyer, K.L. Running, R.D. Huhn, and S.J. Antonia. 2007. Clinical activity and immune modulation in cancer patients treated with CP-870,893, a novel CD40 agonist monoclonal antibody. *J Clin Oncol*. 25:876-883.

Wagner, V., A. Dullaart, A.-K. Bock, and A. Zweck. 2006. The emerging nanomedicine landscape. *Nature Biotechnol*. 24:1211-1217.

Waldmann, T.A. 2003. Immunotherapy: past, present and future. *Nat Med*. 9:269-277.

Walker, L.S.K., and A.K. Abbas. 2002. The enemy within: keeping self-reactive T cells at bay in the periphery. *Nat Rev Immunol*. 2:11-9.

Wolkin, M.V., J. Jorne, P.M. Fauchet, G. Allan, and C. Delerue. 1999. Electronic states and luminescence in porous silicon quantum dots: The role of oxygen. *Phys Rev Lett Rev Lett*. 82:197-200.

Wu, E.C., J.-H. Park, J. Park, E. Segal, F. Cunin, and M.J. Sailor. 2008. Oxidation-Triggered Release of Fluorescent Molecules or Drugs from Mesoporous Si Microplarticles. *ACS Nano*. 2:2401-2409.

Xiao, L., L. Gu, S.B. Howell, and M.J. Sailor. 2011. Porous Silicon Nanoparticle Photosensitizers for Singlet Oxygen and Their Phototoxicity against Cancer Cells. *ACS Nano*. 5:3651-3659.

Yadav, M., and J.S. Schorey. 2006. The beta-glucan receptor dectin-1 functions together with TLR2 to mediate macrophage activation by mycobacteria. *Blood*. 108:3168-3175.

Yang, C.-W., B.S.I. Strong, M.J. Miller, and E.R. Unanue. 2010. Neutrophils influence the level of antigen presentation during the immune response to protein antigens in adjuvants. *J Immunol*. 185:2927-34.

Zammit, D.J., L.S. Cauley, Q.M. Pham, and L. Lefrancois. 2005. Dendritic cells maximize the memory CD8 T cell response to infection. *Immunity*. 22:561-570.

Zhang, L., F.X. Gu, J.M. Chan, A.Z. Wang, R.S. Langer, and O.C. Farokhzad. 2008. Nanoparticles in medicine: therapeutic applications and developments. *Clin Pharmacol Ther*. 83:761-9.

Zhu, G., S.R. Mallery, and S.P. Schwendeman. 2000. Stabilization of proteins encapsulated in injectable poly (lactide- co-glycolide). *Nat Biotechnol*. 18:52-7.